MATERIALS CHEMISTRY
FRONTIERS

REVIEW

View Article Online
View Journal | View Issue

Cite this: *Mater. Chem. Front.*, 2024, **8**, 2197

Enhancing photocatalytic efficiency with hematite photoanodes: principles, properties, and strategies for surface, bulk, and interface charge transfer improvement

Bibhuti Kumar Jha, Sourav Chaule and Ji-Hyun Jang *

Photoelectrochemical cell (PEC) water splitting using hematite as a photoanode has great potential for harnessing solar energy to produce hydrogen. Hematite possesses several advantageous properties, such as abundant availability in nature, eco-friendliness, high photochemical stability, a narrow bandgap (1.9–2.2 eV), and the ability to achieve a theoretical maximum solar-to-hydrogen efficiency of 15.4%. However, its limited light absorption capability, short excited-state lifetime (10^{-6} s), sluggish oxygen evolution reaction kinetics, short hole diffusion length (2–4 nm), and poor electrical conductivity lead to various pathways for electron–hole recombination within the material's bulk, interfaces, and surfaces. These factors significantly restrict the PEC activity of hematite photoanodes. Consequently, extensive research efforts have been dedicated to improving the performance of hematite photoanodes. To enhance the PEC efficiency of hematite, three key aspects require improvement: (I) photon absorption efficiency, (II) charge separation within the semiconductor bulk, and (III) surface charge injection efficiency. This review offers a concise summary of the recent advancements in charge separation research in bulk, surface, and interface studies for water splitting. Furthermore, it provides a comprehensive discussion and summary of the various concepts and mechanisms applied to improve the overall PEC performance of hematite photoanodes.

Received 30th October 2023,
Accepted 18th January 2024

DOI: 10.1039/d3qm01100c

rsc.li/frontiers-materials

1 Introduction

Since the discovery of the photoelectric effect by the French scientist Edmond Becquerel, researchers and engineers have been captivated by the concept of converting light into electrical power or chemical fuels.[1,2] Their aim is to harness the abundant

School of Energy and Chemical Engineering, School of Carbon Neutrality, Graduate School of Semiconductor Materials and Device Engineering UNIST, Ulsan 44919, Republic of Korea. E-mail: clau@unist.ac.kr

Bibhuti Kumar Jha

Bibhuti Kumar Jha, a PhD scholar, completed his Master of Science degree at the Indian Institute of Technology Bombay (IITB), India. Specializing in Energy Science and Engineering, he joined the Department of Energy and Chemical Engineering at UNIST in 2022. Under the mentorship of Professor Jang Ji-Hyun, Bibhuti Kumar Jha is actively engaged in research, with a particular emphasis on photoelectrochemical (PEC) water splitting, Zn-aqueous batteries, and graphitization.

Sourav Chaule

Sourav Chaule is a PhD scholar who earned his Master of Science degree at the Jadavpur University, India. He joined the Department of Energy and Chemical Engineering at UNIST in 2019, where, under the guidance of Professor Jang Ji-Hyun, he focuses his research on photoelectrochemical (PEC) water splitting and solar desalination.

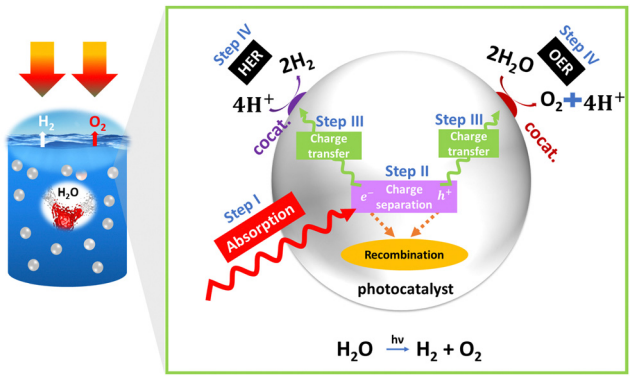

Fig. 1 PEC basics: schematics of overall water splitting.

energy from sunlight and transform it into valuable and strategically significant resources, such as electric power or hydrogen fuel. Leveraging sunlight for hydrogen production and electric power represents a key avenue for sustainable energy development.[3] It aligns with the goals of reducing carbon emissions and enhancing energy storage capabilities, and fosters the establishment of a cleaner and more versatile energy infrastructure.[4,5] In this context, photoelectrochemical water splitting for the production of green hydrogen by utilizing solar energy has gained significant attention in recent years. In 1972, A. Fujishima and K. Honda made a significant discovery involving water splitting using a metal oxide semiconductor (TiO_2).[6] They suggested that water molecules can be decomposed by visible light into oxygen and hydrogen, without the need for any external voltage. This process, known as photocatalysis, involves three main steps.[7] The first step is the absorption of light by the semiconductor. For water splitting to occur, the wavelength of the light must be less than 1000 nm, corresponding to an energy requirement of 1.23 electron volts (eV) (generally, under an air-to-mass ratio of 1.5G).[6] In the second step, the photoexcited charge carriers generated by the absorbed light are separated and migrate to the surface of the semiconductor through diffusion first, followed by a drift mechanism. The final step involves the actual water-splitting reactions, namely the hydrogen evolution reaction (HER) and the oxygen evolution reaction (OER). Fig. 1 provides a more comprehensive illustration of these concepts, and their detailed explanations are elaborated upon below.

Step I: photon absorption

The first step in PEC is the absorption of photons by a photoactive material, typically a semiconductor electrode. The photons transfer their energy to the semiconductor through a process of photon absorption, exciting electrons from the valence band to the conduction band and creating a bound electron–hole pair. To facilitate these reactions, the band positions of the semiconductor play a crucial role, in addition to meeting the band gap requirement ($E_f > 1.23$ eV). For successful water splitting, the conduction band of the semiconductor must have a more negative position than the reduction potential of water, while the valence band should be more positive than the oxidation potential of water. These band positions allow for the efficient transfer of electrons and holes to facilitate the desired reactions.

Step II: charge separation

In PEC, efficient separation of excitons is necessary to prevent recombination. More efficient separation can occur by creating the built-in potential within the semiconductor or by introducing a separate electron and hole acceptor. Photon absorption can be affected by several properties of semiconductors such as band gap and their nature (direct/indirect), band position, absorption coefficient, optical penetration length, refractive index, *etc*.

Step III: charge transfer

Once the excitons are separated, the free electrons and holes diffuse through the semiconductor material. Diffusion allows the charge carriers to move from regions of higher concentration to lower concentration, enabling efficient transport towards the electrode–electrolyte interface. After diffusion, the charge carriers undergo drift, propelled by either an applied electric field or the built-in potential within the semiconductor. Drift transport facilitates the movement of the charge carriers toward their respective electrodes, ensuring effective charge collection and preventing recombination. The properties of semiconductors, including parameters such as exciton binding energy, effective carrier mass, carrier lifetime, carrier mobility, dielectric constant, diffusion length, conductivity, resistivity, space charge layer, depletion width, flat band potential, and surface states, significantly influence charge separation in semiconductor-based materials. Efficient charge separation is a critical factor in enhancing the overall efficiency of PEC systems, as it directly impacts catalytic activity.

However, it is important to note that these semiconductor properties can also lead to the recombination of charge carriers, particularly excitons, within the bulk material. This recombination process can detrimentally affect the overall

Ji-Hyun Jang

Prof. Ji-Hyun Jang completed a PhD in Chemistry from the Korea Advanced Institute of Science and Technology (KAIST) in 2003. Following her doctoral studies, Professor Jang served as a postdoctoral fellow in the United States, at the Massachusetts Institute of Technology (MIT) from 2004 to 2009. In 2009, she joined the Ulsan National Institute of Science and Technology (UNIST), Korea, as a faculty member. Her research endeavors focus on diverse areas, including photoelectrochemical water splitting, solar desalination, Zn-aqueous batteries, lithography, and supercapacitors. Currently, Professor Jang holds the position of associate editor for the Journal of Materials Today Energy.

efficiency of a PEC system. Additionally, recombination events may occur at various interfaces, such as the substrate–electrode, electrode–catalyst, and electrode–electrolyte interfaces.

Addressing these recombination processes and modifying the semiconductor properties to minimize them is a key area of study in PEC systems. Specifically, we will delve into the details of these recombination phenomena and explore strategies for mitigating their impact to enhance the performance of semiconductor-based PEC systems.

Step IV: catalytic process

At the interface between the electrode and the electrolyte in a PEC system, pivotal catalytic processes transpire. In this context, photoexcited electrons participate in the reduction of a redox species residing within the electrolyte, while the generated holes undertake the oxidation of another species. These catalytic reactions serve as the cornerstone for harnessing solar energy and facilitating essential chemical transformations, such as water splitting or CO_2 reduction. Notably, the role of the electrode–electrolyte interface in these processes cannot be understated. The properties of the electrolyte in this context wield substantial influence. Parameters such as pH, the extent of the ohmic drop (iR drop), viscosity, effective ion size, and activity coefficient play pivotal roles in shaping the kinetics of these catalytic reactions. Additionally, the properties of the catalyst, including its electrocatalytic characteristics, exchange current density, and charge transfer resistance, are of paramount importance in catalyzing these reactions effectively. Furthermore, the interface established between the semiconductor and the electrolyte is of paramount significance for facilitating charge transfer and efficient chemical reactions. This interface must exhibit desirable attributes such as an ample surface area, specific morphology, appropriate chemical composition, potential inclusion of catalysts or co-catalysts, high electrical conductivity, energy levels conducive to efficient charge transfer, and stability when subjected to the operational conditions of the PEC cell. Skillful engineering of this interface serves to minimize energy losses and optimize the overall efficiency of the PEC system.

To achieve practical application, the solar-to-hydrogen conversion (STH) efficiency needs to exceed 10%, equivalent to a hydrogen production rate of 154 μmol H_2 cm^{-2} h^{-1}. A semiconductor material with a band gap ranging from 1.8 to 2.0 eV ($\lambda \sim$ 600–700 nm) is capable of absorbing photons at a rate of approximately 260 nm^{-2} s^{-1}. This absorption rate leads to a photocurrent density of 8.3 mA cm^{-2}.[8] Hematite (α-Fe_2O_3) meets these criteria as it exhibits a high theoretical photocurrent density of 12.6 mA cm^{-2} under an air-to-mass ratio of 1.5G, resulting in STH ~15.4%.[9,10] Therefore, hematite is considered one of the most promising photoanode materials for PEC water splitting. Its advantages include abundance, stability, a suitable bandgap, and environmentally friendliness.[11] Despite extensive investigations into alternative photoanodes such as $BiVO_4$[12–14] and WO_3,[15,16] challenges including severe hole transport limitations in $BiVO_4$ and a comparatively large bandgap in WO_3 have been observed, restricting their light absorption.[17,18]

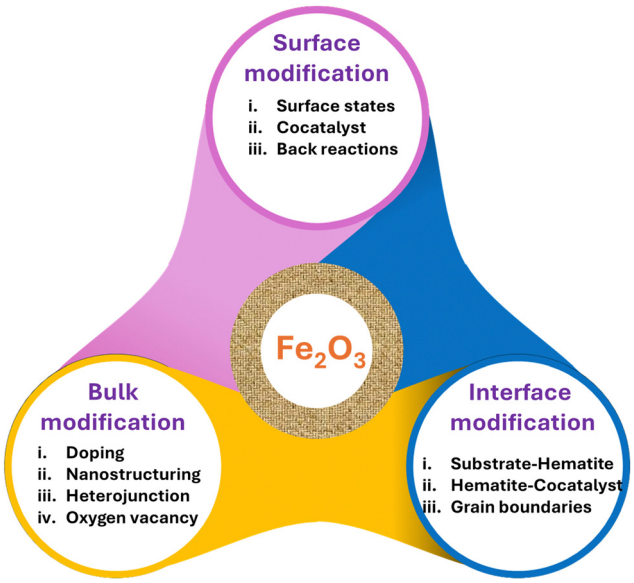

Fig. 2 Schematic depicting the perspectives of the review.

Other photoanodes, for instance $BiVO_4$, have achieved reported current densities of 6.12 mA cm^{-2} (Z. Tian *et al.*[19]), reaching their theoretical value, and hematite retains substantial untapped potential, presenting an avenue for further scientific exploration to approach its theoretical limits.[20] Therefore, hematite is preferred over other photoanodes for PEC water splitting due to its unique properties and advantages. However, hematite suffers from two main problems: (I) poor carrier transport and separation, and (II) a sluggish OER. The challenge leading to inadequate carrier transport and separation arises from a disparity between the penetration depth of light (ranging from 120 to 46 nm within the wavelength range of approximately 550 to 450 nm) and the limited hole diffusion length (which falls between 2 to 4 nm). This mismatch impedes the efficient migration of holes towards the surface, where they are intended to participate in the OER, as they tend to recombine with electrons before reaching the surface.[21,22]

Numerous review papers have been published on strategies aimed at enhancing the overall efficiency of hematite. This review focuses primarily on mitigating the rate of charge carrier recombination by improving charge transfer in both bulk and interfaces, including substrate–hematite, hematite–cocatalyst, and cocatalyst–electrolyte interactions. The scope of this review paper encompasses the following aspects: first, it starts with basic principles by covering historical background and working principles, followed by the different characterizations needed for finding suitable materials. The next section discusses hematite as a photoanode, including basic properties such as surface states, charge transfer, trapping, and recombination in hematite. Additionally, the proposed mechanism behind the OER of hematite is discussed. In the subsequent section, different strategies (Fig. 2) to improve bulk charge transfer, surface charge transfer, and interfacial charge transfer are reviewed before concluding.

2. Characterization techniques for PEC electrode evaluation

Characterization techniques offer the scientific foundation for the obtained performance. They are indispensable for elucidating the structure, composition, and performance of materials used in PEC systems. This knowledge is critical for advancing the design and optimization of photoelectrodes, ultimately enhancing the efficiency and viability of solar-driven water-splitting technologies for sustainable energy production.[23] The choice of characterization techniques depends on the specific materials and systems you are working with. Here are some of the most commonly used techniques in PEC electrode evaluation.

Photocurrent–voltage (*I–V*) measurement

This is a fundamental test to assess the PEC performance of an electrode. Two of the most important considerations are the onset potential and photocurrent density. It involves measuring the photocurrent generated by the electrode as a function of applied voltage (potential). This helps determine key parameters such as the short-circuit current, open-circuit voltage, and fill factor, which are crucial for assessing device efficiency. The *I–V* curve measurement, both with and without light illumination, is used to determine the photocurrent and efficiency of the PEC electrode.[24,25]

Electrochemical impedance spectroscopy (EIS)

EIS is used to study charge transfer and mass transport processes at the electrode–electrolyte interface. It reveals information about electron and ion transport kinetics, as well as the interfacial charge transfer resistance, making it a valuable tool for optimizing PEC cell design.[26–28]

Mott–Schottky analysis

A Mott–Schottky plot is a graph of the inverse of the capacitance of a semiconductor/electrolyte junction as a function of the applied voltage. The plot is typically linear, and the slope of the line can be used to determine system properties such as the flat-band potential, carrier density, charge carrier type, doping level, PEC response kinetics, operational parameters, as well as carrier density, capacitance, and impedance of semiconducting electrodes.[29–32]

Transient absorption spectroscopy (TAS)

TAS measures the dynamics of photoexcited carriers in PEC materials, providing insights into carrier recombination rates, trap states, and carrier lifetime. This information is valuable for designing suitable photoelectrodes.[33] When combined with Mott–Schottky analysis, which determines flat-band potential and carrier density, it offers a comprehensive understanding of the semiconductor's electronic structure and the dynamics of photoexcited carriers, including recombination processes and trap states.

Steady-state and time-resolved photoluminescence (PL)

PL spectroscopy is employed to study the radiative recombination of charge carriers in PEC materials, offering insights into material quality and non-radiative recombination pathways. PL intensity and lifetime provide data on charge carrier concentration and mobility, while the spectra shape informs about the size, shape, and composition of nanomaterials.[34]

UV-Visible spectroscopy

UV-Vis spectroscopy is used to measure the optical properties of PEC materials, such as absorbance and bandgap energy. The combination of UV-Vis and PL spectroscopy characterization techniques can provide valuable information about the electronic structure, optical properties, and recombination processes of materials. This information can be used to optimize the design of photoelectrodes for water-splitting applications.[35,36]

3. Optoelectronic properties of hematite

3.1. Light-matter interactions in hematite nanomaterials

The optical absorption properties of hematite have been extensively investigated.[37–40] Hematite exhibits distinct absorption characteristics spanning a wide spectrum.[40] Broadly, α-Fe_2O_3 exhibits two absorption peaks within the wavelength range of 200–800 nm.[41] The first peak, occurring at 400 nm, is attributed to transitions from nonbonding O 2p orbitals to vacant conduction band Fe^{3+} 3d orbitals ($O_{2p}{}^{2-} \rightarrow Fe_{3d}{}^{3+}$). This transition is responsible for the strong absorption observed at that wavelength. The second peak, appearing at 590 nm, arises from indirect transitions between the valence band edge Fe^{3+} 3d orbitals and vacant conduction band Fe^{3+} 3d orbitals ($Fe_{3d}{}^{3+} \rightarrow Fe_{3d}{}^{3+}$), resulting in a weaker absorption.

One limitation of hematite is its relatively low absorptivity near the bandgap.[42] As a result, in order to achieve high absorption performances, it is necessary to synthesize thick hematite films. These films absorb a substantial portion of the incident light to compensate for the low absorptivity and maximize the PEC performance. However, as the thickness of the materials increases, the recombination rate also increases. Therefore, determining the optimum thickness is crucial to achieving high performance.

Absorption of light results in charge carrier generation called photogenerated charge carriers. Their lifetime is essential for charge separation. The efficiency of a photoelectrode for water splitting relies on the effective transport of photogenerated minority charges to the semiconductor–electrolyte junction, enabling high conversion efficiency.[43] Hematite nanoparticles exhibit rapid nonradiative processes and low fluorescence quantum yields on the order of 10^{-5}, thereby limiting the lifetime of the excited state.[44] Studies using femtosecond laser spectroscopy reveal fast dynamics, with nanomaterials decaying within 8 picoseconds.

Research conducted on epitaxially grown thin films with a thickness of 100 nm, utilizing oxygen plasma-assisted molecular beam deposition, has demonstrated a reduced impact from both bulk and surface defect states compared to nanoparticle-based systems. In epitaxially grown thin films, hot electron relaxation occurs within 300 femtoseconds,[43] followed by

recombination within 3 picoseconds. The primary mechanism responsible for carrier trapping is attributed to mid-gap Fe^{3+} d–d states located approximately 0.5–0.7 eV below the conduction band edge, exhibiting an optical transition energy of approximately 1.5 eV.[43,45] These findings highlight the impact of carrier trapping, low mobility, and short photogenerated lifetime on the hematite's performance as a water-splitting photoelectrode.[43]

3.2. Charge carrier dynamics and transport in hematite nanostructures

There are different types of transitions that occur in hematite upon irradiation. These transitions can be categorized into four types (Fig. 3a): (a) single ligand field (LF) transitions, (b) pair LF transitions, (c) ligand-to-metal charge transfer (LMCT), and (d) metal-to-metal charge transfer (MMCT). The first two transitions, single LF and pair LF, do not generate electron–hole pairs. Therefore, we will not discuss them further in this context. For more detailed information on these transitions, please refer to other sources.[46,47]

Among these transitions, the LMCT transition is widely recognized as the primary, and sometimes the sole, source of photocurrent. It plays a crucial role in determining the photoelectrochemical properties of hematite. The reaction associated with this LMCT transition is as follows:

$$Fe^{3+} + O^{2-} \rightarrow Fe^{2+} + O^{-}$$

Upon excitation, the electron is located in an Fe 3d orbital, while the hole is present in an O 2p orbital (Fig. 3b), which is crucial for water oxidation activity.

On the other hand, the MMCT transition involves the transfer of an electron from one Fe site to another, resulting in the splitting of valence states. This electron transfer process can be represented by the following reaction:

$$2Fe^{3+} \rightarrow Fe^{2+} + Fe^{4+}$$

In this scenario, excitation results in the generation of a hole in an Fe 3d orbital. Both the LMCT and MMCT transitions play significant roles in the electron conduction properties of hematite. The LMCT transition facilitates electron hopping between O^{2-} and Fe^{3+} ions, contributing to electron conduction within the material. On the other hand, the MMCT transition leads to charge disproportionation, involving the transfer of electrons between different Fe sites. These transitions, LMCT and MMCT, are responsible for the observed electron transport behavior in hematite.

Previous studies disregarded the involvement of MMCT in solar water splitting.[48] However, recent research utilizing near-edge X-ray absorption fine structure (NEXAFS) spectroscopy during *in situ* PEC cell experiments has provided evidence of its significant contribution to the photocurrent.[49] NEXAFS analysis of the illuminated hematite film revealed two distinct pre-edge peaks in the spectra, representing electron transitions from the O 1s core level to either O 2p hole states *via* the charge transfer band (t_{1u}^{CTB}) or Fe 3d hole states *via* the upper Hubbard band (a_{1g}^{UHB}), in addition to the main edge corresponding to transitions to conduction band (CB) levels. These hole states, with a separation of approximately 1.3 eV, exhibit activity for charge transfer and become prominent only at applied potentials near and above the photocurrent onset potential. TAS results indicate rapid bulk recombination, with a significant loss of holes within 1 ns. Consequently, only the remaining holes migrating to the surface can be detected by NEXAFS. The combined spectral weight distribution of CTB and UHB peaks demonstrates a peak near the onset potential, resembling the surface capacitance (often referred to as trap states capacitance) measured using photoelectrochemical impedance spectroscopy.

3.3. Band bending effects on charge carrier dynamics

When two regions with different Fermi levels are brought into contact, the Fermi level tends to equalize due to the diffusion of charge carriers (electrons or holes) across the interface. This equalization process leads to a bending of the energy bands near the junction, resulting in band bending (Fig. 4a and b).[50] Band bending is beneficial as it promotes charge separation and transport, and this effect can be further enhanced by doping, nanostructuring, external bias, *etc.*[51]

Overall, the band bending of a semiconductor occurs because the surface charge-induced electric field is not

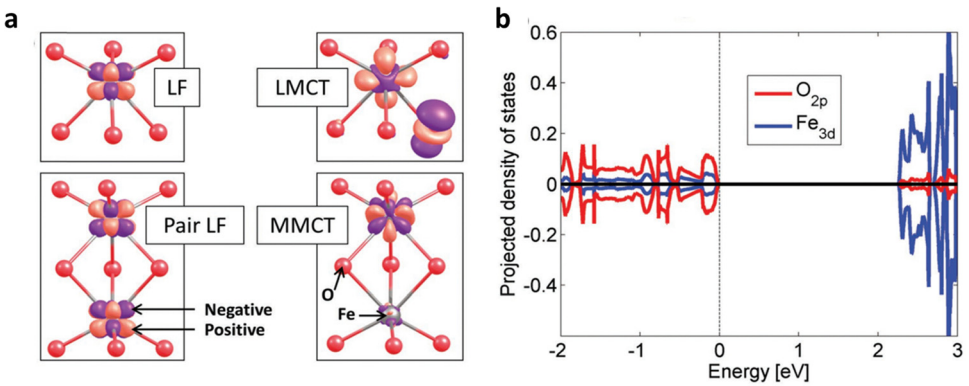

Fig. 3 Charge transfer in hematite photoanodes. (a) Four different types of charge transfer LF, pair LF, LMCT, and MMCT. (b) Dominant orbitals involved in charge transfer. Reproduced from ref. 47 with permission from John Wiley and Sons, copyright 2018.

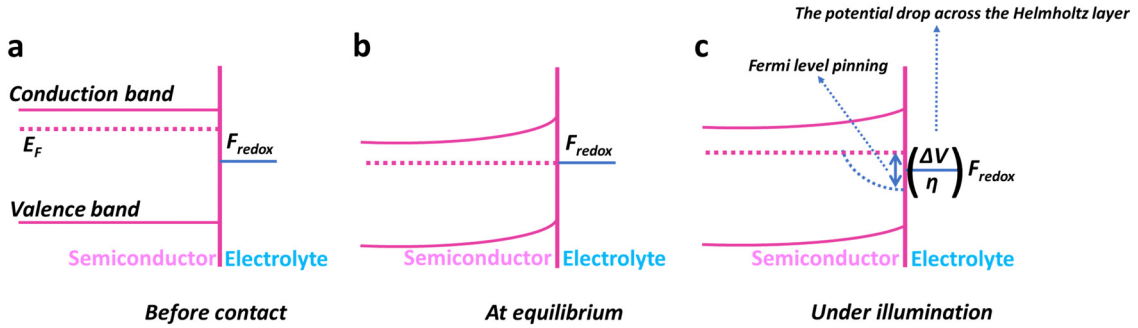

Fig. 4 Semiconductor–electrolyte interfaces. (a) Band structure of an n-type semiconductor before contact with the electrolyte. (b) Under equilibrium conditions, a dominant redox pair affects electrochemical potentials (band bending). (c) Illumination causes a downward-bent quasi-Fermi level for photogenerated holes (Fermi-level pinning).

effectively screened due to the semiconductor's low concentration of free carriers.[50] The formation of a space charge region near the surface of the semiconductor leads to alterations in its physical properties. These changes encompass variations in the energy band structure, free carrier density, and local conductivity within the space charge region, distinguishing it from the bulk of the semiconductor. Consequently, the chemical properties of the semiconductor are also influenced by these modifications.[52]

3.4. Surface states and their impact on optoelectronic behavior

The term "surface state" refers to the electronic states present at the surface of the material. The surface of hematite photoanodes plays a critical role in the performance of the PEC cell because it affects the transfer of charge carriers (electrons and holes) during the water-splitting process and, to some extent, the absorption of light.[53] Surface states in hematite arise due to the imperfections, defects, and impurities present on the surface of the material. These states can trap charge carriers, leading to increased recombination and reduced efficiency of the PEC cell.[52] Surface states can affect the band bending and charge transfer kinetics, and cause Fermi-level pinning,[50] at the interface between the hematite photoanode and the electrolyte. The Fermi-level pinning (Fig. 4c) causes a reduction in photovoltage. Sometimes, it can even dominate fast charge transfer kinetics. An example of this can be found in the work of Yang *et al.*,[54] who sought to enhance charge transfer by decorating MnOx on hematite. However, the presence of Fermi-level pinning hindered the anticipated enhancement in overall performance.

3.5. Optical transitions: size and shape insights

The color of hematite nanostructures is influenced by several factors including phase, size, and shape. Studies show that different sizes and shapes result in varying colors, ranging from maroon to purple.[55] Specific surface planes exhibit varying reflectance abilities, which affect the intensity of reflection across different wavelengths and determine the apparent color.[56] The optical properties of hematite are analyzed using techniques such as diffuse reflectance spectroscopy, revealing an approximate band gap of 2.2 eV and various ligand field transitions.[57] Hematite nanoparticles demonstrate size-dependent absorption, with smaller particles exhibiting a blue shift in absorption.[40] Furthermore, the optical properties of hematite structures are influenced by their shape, leading to shape-induced shifts in absorption bands. These color and optical variations result from factors such as finite size effects and anisotropic effects governed by dipole and electric field distributions.[57]

3.6. Correlation between photoluminescence and structural properties

In bulk Fe_2O_3, photoluminescence is typically absent due to forbidden d–d transitions and efficient lattice and magnetic relaxations.[58] However, in nanostructured hematite materials, photoluminescence can be observed due to size-dependent optical properties and the phenomenon of quantum confinement.[58,59] Nanostructures, through the effect of quantum confinement, alleviate constraints on forbidden d–d transitions, enabling partial optical transitions. Additionally, the increased 3d–4sp hybridization in nanoparticles weakens magnetic relaxations within hematite, leading to long-lived excited states. This effect is attributed to the relaxation of magnetic constraints.[60] Furthermore, local lattice distortion and a collapse of the Fe magnetic moment in hematite nanoparticles can contribute to luminescence upon photoexcitation.[60] Zou *et al.*[60] reported strong photoluminescence in hematite nanoparticles with sizes smaller than 20 nm, whether in the form of a hydrosol suspended in water or organosol-capped nanoparticles with surfactants suspended in toluene. In water, the dominant emission occurred around 575 nm, corresponding to the band-edge emission, while capped nanoparticles exhibited broader Gaussian-fit emissions around 590 nm. The shift in emission wavelength was attributed to the stronger 3d–4sp hybridization in capped nanoparticles in toluene compared to nanoparticles in water. Additionally, Cherepy *et al.*[61] observed an emission band at 400 nm (excited at 300 nm) in spindle-shaped hematite nanostructures with dimensions around 1–5 nm. This emission, occurring above the bandgap energy of hematite, was rarely detected and was attributed to LMCT transitions.

These examples underscore the interconnection between the absorption and emission properties of hematite and their dependence on size and morphology. The absorption bands of hematite, spanning from ultraviolet (UV) to near-infrared

(IR) wavelengths, are associated with various transitions, including Fe^{3+} ligand field transitions, pair exciton transitions, and LMCT transitions. The quantum size effect exhibited by hematite nanostructures leads to notable alterations in their absorption and photoluminescence characteristics.

3.7. Band structure

The bandgap of hematite, which represents the energy difference between the valence and conduction bands, is an important characteristic.[62] The calculated bandgap (Fig. 5) for α-Fe_2O_3 is typically found to be around 2.1 eV.[63]

The electronic band structure reveals the allowed energy states and their dispersion throughout the Brillouin zone. It shows that the valence band maximum is primarily composed of oxygen 2p orbitals, while the conduction band minimum is dominated by iron 3d orbitals.[64] The band structure also indicates the presence of other bands and energy levels associated with specific electronic transitions.

The electronic band structure of hematite is influenced by its crystal structure, which is characterized by a rhombohedral arrangement. The symmetry and arrangement of atoms in the crystal lattice affect the band structure, resulting in the formation of bandgaps and energy bands with specific characteristics.

Understanding the electronic band structure of hematite is crucial for interpreting its optical properties, such as absorption and emission spectra. The band structure provides information about the energy levels involved in electronic transitions and helps explain phenomena such as the absorption of light and the generation of photocurrents.

4. Water splitting mechanism of hematite

The water oxidation reaction is a proton-coupled electron transfer process, but its detailed mechanism remains incompletely understood. In most kinetic models, the rate-determining step (RDS) is considered to be the formation of the O–O bond. This step involves two pathways: water molecule nucleophilic attack (WNA) and radical coupling (I2M). However, the sluggish kinetic activity of hematite photoanodes used in PEC water oxidation poses a significant limitation in hole injection efficiency. Extensive research efforts have been dedicated to unraveling the reaction mechanism involved in PEC water oxidation.

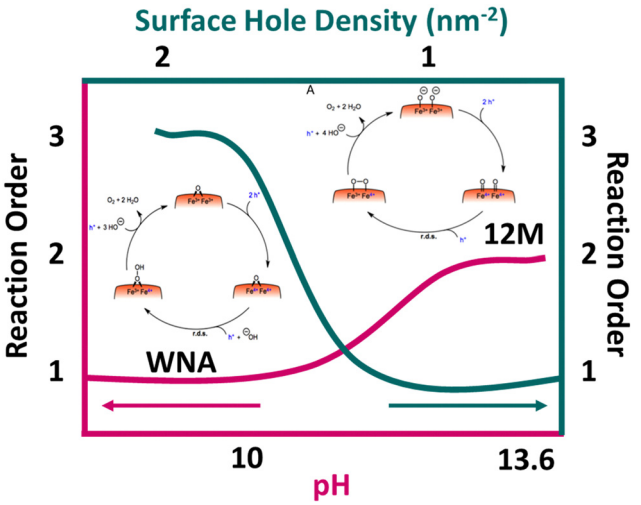

Fig. 6 Mechanism: factor affecting the rate of water splitting on hematite.

Rate law analysis is valuable for investigating hematite photoanodes in water oxidation because it provides mechanistic understanding, quantifies reaction kinetics, estimates surface hole density, reveals transition mechanisms, and elucidates pH dependence. In their study on the order of water oxidation on a hematite photoanode, Formal *et al.*[65] conducted a rate law analysis. They estimated the surface hole density by analyzing the photoinduced absorption spectroscopy signal at 650 nm. The results revealed that at a low accumulated hole density, the reaction proceeded slowly and followed first-order kinetics. However, as the surface accumulated hole density increased to a level sufficient for the oxidation of nearby metal atoms, a faster and third-order mechanism replaced the original first-order reaction (Fig. 6). This transition mechanism, which depends on the accumulated hole density on the surface, was discovered for the first time. In a subsequent study by Zhang *et al.*,[66] the reaction pathways of hematite for water splitting were investigated under different pH conditions. Poor activities were observed in the pH range of 7 to 10. However, following the Nernstian trend (approximately 59 mV pH^{-1}), as the pH increased, the onset potential gradually decreased, while the photocurrent

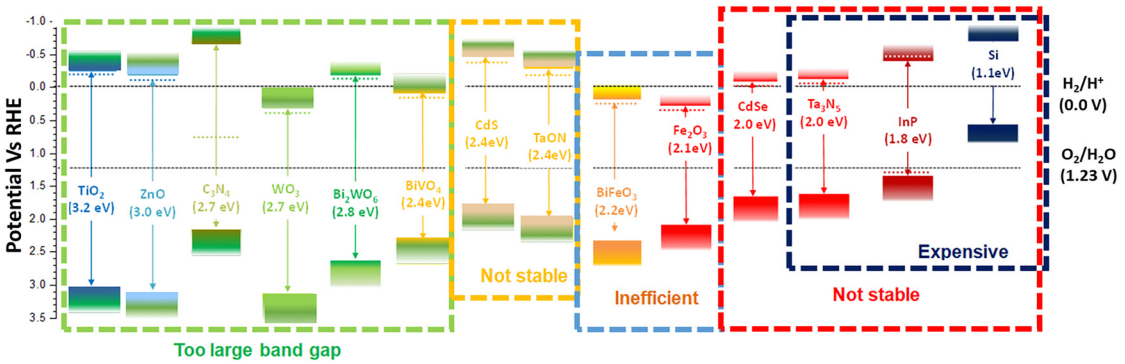

Fig. 5 Band characteristics: band position and band gaps of different photocatalysts.

density continued to increase. The authors also examined the kinetic isotope effect (KIE) value, which exhibited a significant downward trend from pH 7 to 13.6 at 0.9–1.2 V (*vs.* RHE). KIE ranged from 1.5–3.1 at pH 9–11 and approached 1 at pH 13 or higher.[67] This suggested that the RDS did not involve proton transfer under strongly alkaline conditions. Furthermore, the authors determined the reaction orders of hole transfer to be 1.1 and 2.4 at pH values of 10 and 13.6, respectively (Fig. 6). Based on these findings, the authors proposed that the reaction pathways were pH-dependent. The WNA reaction pathway exhibits a preference for near-neutral electrolytic conditions, while the 12 M-based mechanisms tend to favor high alkaline environments (pH 13.6) (Fig. 6). Fig. 6 concludes that upon increasing the pH value the order of reaction increases and the same trend is observed for surface hole density.

Based on the rate law analyses by Formal *et al.*[65] and Zhang *et al.*,[66] it is evident that the carrier density and pH of the electrolyte influence the mechanism and, consequently, the kinetics of PEC water splitting. Therefore, we can conclude that any modification affecting the electronic states or charge separation efficiency of hematite will impact the mechanism of water-splitting.

5. Strategies for charge separation modification in the bulk, surface, and interface

Hematite is a potential photoanode for practical PEC applications. However, it suffers from poor charge carrier mobility and a short diffusion length of photogenerated charge carriers, which limits its overall performance. There are many strategies that have been applied to improve charge separation including nanostructuring, doping, co-catalyst, *etc.*[68–72] These charge separation modification techniques aim to reduce the recombination rate of charge carriers, extend their diffusion length, and improve their collection at the respective electrodes. By enhancing charge carrier dynamics, the efficiency and performance of hematite photoanodes for PEC water splitting can be significantly improved.

STH is the common way to report the performance of a PEC electrode. STH efficiency is the product of absorption efficiency, charge separation efficiency in bulk and charge separation efficiency of the surface and interface. In this section, different ways to improve surface, bulk, and interface efficiency are reported. Formulae for calculating the efficiencies are mentioned below.

$$\mathrm{IPCE}(\lambda) = \mathrm{EQE}(\lambda) = \frac{\text{electrons per cm}^2\ \text{s}^{-1}}{\text{photons per cm}^2\ \text{s}^{-1}} = \frac{\left|J_{\mathrm{H_2O}}\left(\text{mA cm}^{-2}\right)\right| \times 1239.8(\text{V} \times \text{nm})}{P_{\text{mono}}(\text{mW cm}^{-2}) \times \lambda(\text{nm})} \quad \text{(I)}$$

$$\mathrm{STH}\ (\%) = \left[\frac{J_{\mathrm{H_2O}}\left(\text{mA cm}^{-2}\right) \times (1.23\ \text{V}) \times \eta_{\mathrm{F}}}{P_{\text{Total}}(\text{mW cm}^{-2})}\right] \quad \text{(II)}$$

$$\mathrm{STH}\ (\%) = \left[\frac{\text{Chemical energy produced}}{\text{Solar energy input}}\right] = \left[\frac{\text{Rate of H}_2\text{ production} \times \Delta G_{\mathrm{H_2O}\rightarrow\mathrm{H_2}+0.5\mathrm{O_2}}}{\text{Total incident solar power} \times \text{Electrode area}}\right] \quad \text{(III)}$$

$$\eta_{\mathrm{STH}} = \eta_{\mathrm{Abs}} \times \eta_{\mathrm{bulk}} \times \eta_{\mathrm{surface}} \quad \text{(IV)}$$

5.1. Modification of bulk charge separation efficiency

Theoretical calculations suggest that hematite has the potential to achieve a maximum photocurrent of 12.6 mA cm^{-2} when absorbing light at a wavelength of 600 nm under AM 1.5 G solar irradiation conditions (Fig. 7a).[73] However, current state-of-the-art hematite photoanodes have not reached this theoretical limit, even with high positive electric bias that achieves a surface hole injection efficiency of 90%.[74,75] The limited carrier mobility (on the order of 10^{-2} cm^2 V^{-1} s^{-1}) and short carrier lifetime (picoseconds) contribute to the short diffusion distance of holes (2–4 nm) within hematite.[76] This indicates that the majority of holes recombine with electrons in the bulk before reaching the surface space charge layer, leading to low internal quantum efficiency or absorbed photon-to-current efficiency (APCE).

Carrier transport and ground-state mobility in metal oxide photocatalysts, including hematite, are determined by small polaron hopping.[76] In the presence of displaceable ions, an electronic charge carrier can minimize its energy by localizing and becoming self-trapped when approaching a Fe center. Phonon motion enables the charge carrier to hop between atoms when two Fe centers are in proximity. Recent investigations have shown that small polaron formation strongly influences the photoconversion efficiency of hematite photoanodes.[77] Near the band edge, photoexcited carriers in hematite tend to be localized as small polarons, leading to lower excited-state mobility and shorter carrier lifetimes. As the excitation energy increases, more mobile carriers and fewer polarons are formed due to the creation of additional optical phonons (Fig. 7b). The increased hopping rate of the polaron, facilitated by the non-thermal phonon bath, results in improved excited-state carrier mobility and longer carrier lifetimes (Fig. 7c and d). Interestingly, these trends align with the APCE of hematite (Fig. 7e), indicating that lower photoconversion efficiency occurs at wavelengths where small polaron formation is prevalent and the small polaron's hopping rate is low.

5.1.1. Nanostructuring. Creating distinctive nanostructures is seen as an effective method to reduce the distance between the material's bulk and its surface, while also potentially optimizing photon absorption efficiency (there is a trade-off).[78] One-dimensional (1D) materials, such as nanowires and nanorods, are commonly employed due to their dimensions, which are similar to carrier diffusion lengths, leading to enhanced effectiveness (Fig. 8a).[79,80] A highly refined hematite nanowire array with an ultrafine diameter of approximately 10 nm was successfully fabricated.[81] The PEC results demonstrate that the ultrafine

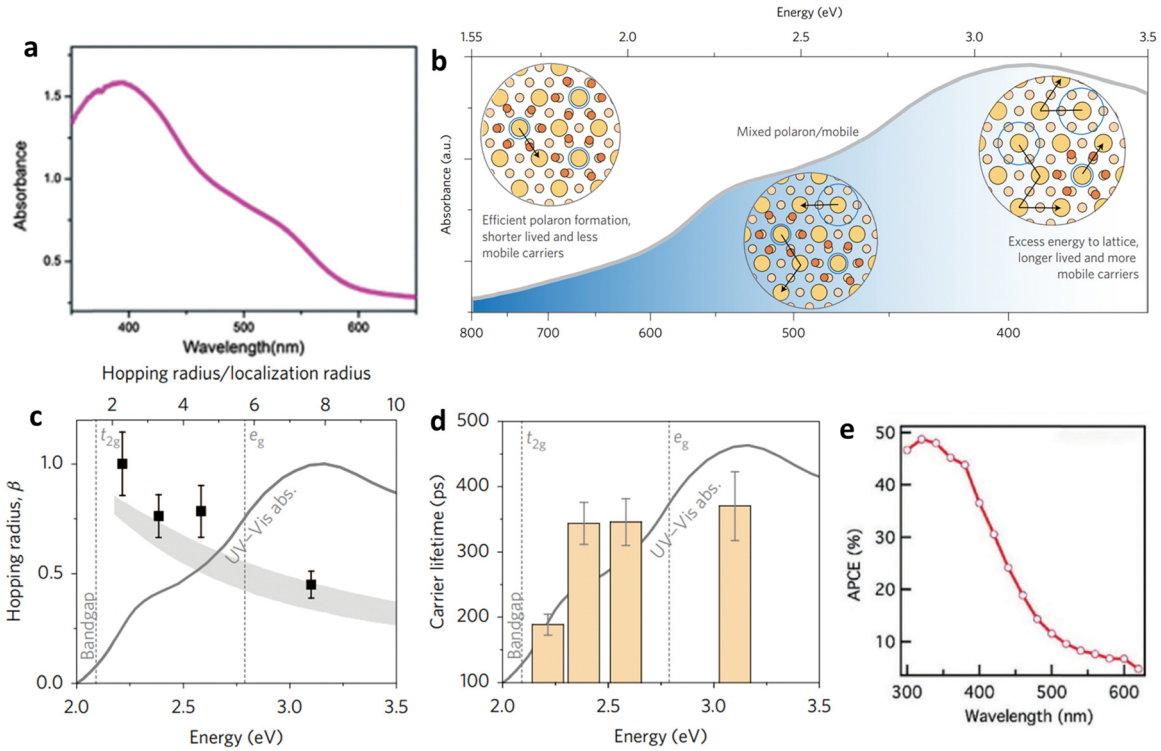

Fig. 7 Impact of light absorption on carrier dynamics and efficiency. (a) Polaron formation and the impacts of hematite's absorption wavelength. (b) Variation of internal quantum efficiency (APCE) of a planar Fe_2O_3 photoanode with wavelength. (c) Wavelength-dependent characteristics of hematite are investigated, specifically regarding $Fe_2O_3/TiSi_2$ film, by analyzing its absorption spectrum. (d) and (e) Formation and decay of small polaron states in the excited state of hematite were studied in terms of energy dependence. The excited-state lifetime of charge carriers in hematite was experimentally measured. The impact of polaron formation on hematite's absorption was also examined. It was observed that at excitation wavelengths close to the band edge, efficient polaron formation occurred, resulting in the trapping of excited-state carriers and faster recombination. As the excitation energy increased, the efficiency of excited-state polaron formation decreased, leading to an increased presence of nonthermal phonons. This, in turn, facilitated greater polaron hopping, resulting in enhanced mobility and longer lifetime for the excited-state carriers. Reproduced from ref. 77 with permission from Springer Nature, copyright 2017.

hematite nanobundle photoelectrodes exhibit superior efficiencies in charge separation compared to the nanorod photoelectrodes (Fe_2O_3 NRs) (Fig. 8b). The improved charge separation efficiency can be partially attributed to the reduced charge transfer distance resulting from the 1D nanowire structure. A reduction in particle size also leads to an increase in charge carrier density. For example, a nanoporous hematite electrode with mesocrystal superstructures and nanoparticles, averaging approximately 5 nm in size, exhibited a better performance in PEC water splitting. This improvement can be attributed to the reduced charge transport distance to the surface and the enhanced charge carrier density, as shown in Fig. 8c.[82] Another strategy for enhancing charge transfer through nanostructuring involves branching the nanoroads, effectively reducing hole drift distances (Fig. 8d).[83] A hierarchical branched array of Fe_2O_3 nanorods (BNR) demonstrated higher photocurrents and improved charge separation efficiencies when compared to bare Fe_2O_3 nanorod photoelectrodes. This improvement can be attributed to the hierarchical structure of the Fe_2O_3 BNRs.

Furthermore, Jang *et al.* presented a straightforward solution-based approach for creating porous electrodes, as detailed in Fig. 8e.[84] This approach resulted in a remarkable 450% enhancement in performance when compared to previously reported Si:Ti-doped hematite. The porous electrode structure offers a substantial increase in surface area for reaction processes and reduces the migration distance for charge carriers. Consequently, this leads to a lower recombination rate, ultimately resulting in significantly improved performance in PEC applications.[85–87]

5.1.2. Doping. Incorporating heteroatoms into hematite through doping can significantly enhance carrier mobility and density.[88] By improving carrier mobility (resulting in a faster drift velocity within the built-in field) and density (increasing band bending and intensifying the built-in field), the doping process can effectively reduce recombination. N-type doping, which involves the substitution of Fe^{3+} ions with tetravalent and pentavalent ions, is commonly employed to achieve this. This type of doping leads to an increase in donor density. Importantly, the heightened carrier density can enhance band bending at the interface between the semiconductor and electrolyte.

In recent years, metal (Sn, Ti, Zr, *etc.*) doping has been commonly employed to modify hematite.[89–93] The impact of Ti and Sn (unintentionally doped) co-doping on the bulk charge efficiency of hematite is investigated (Fig. 9a).[94] Their findings revealed that the high and uniform content of Sn in Ti-doped

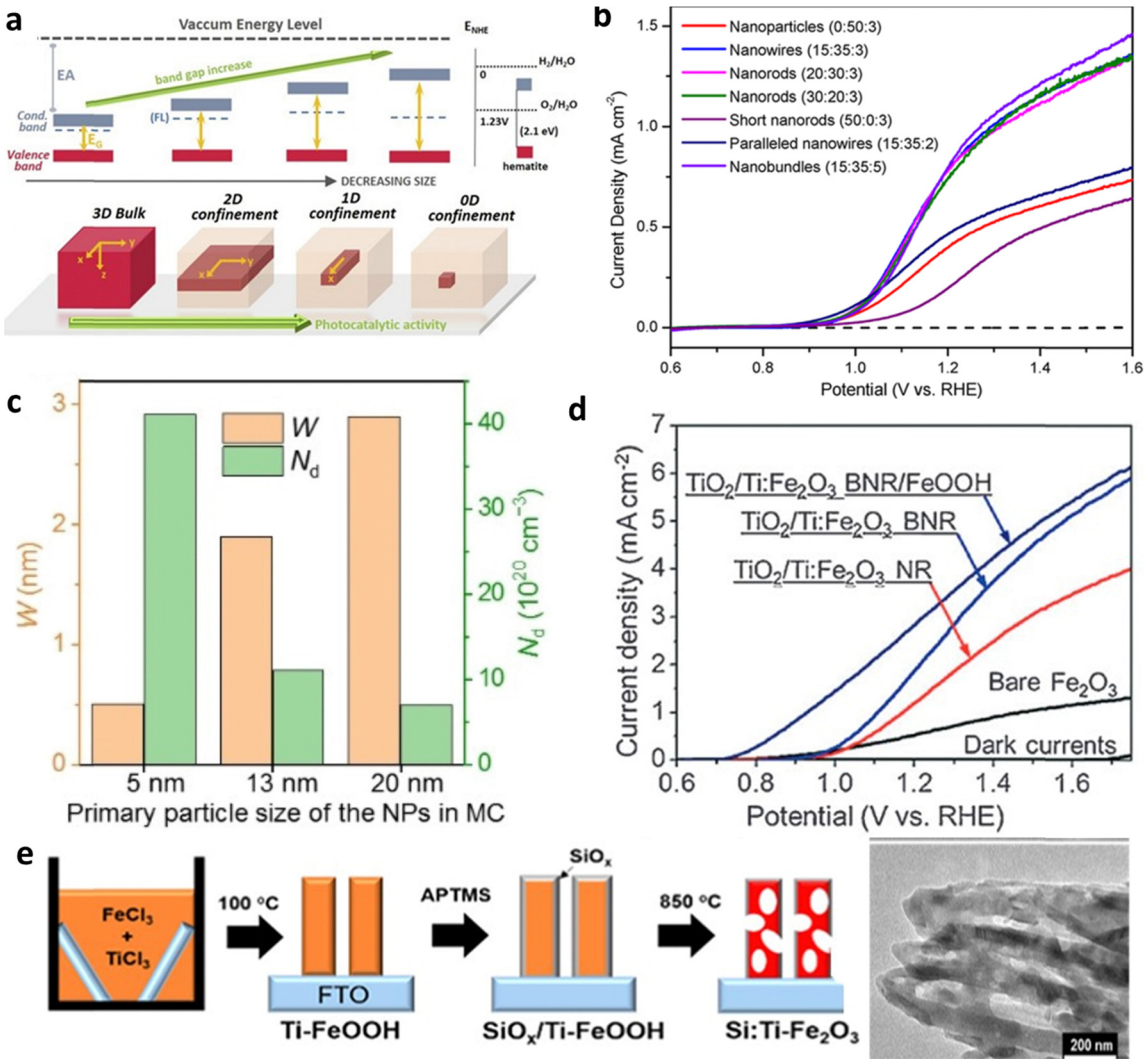

Fig. 8 Impact of nanostructuring and morphology. (a) Effect of particle size on bandgap and photocatalytic activity. Reproduced from ref. 79 with permission from APL Materials, copyright 2020. (b) *J*–*V* curve analysis of different nanostructured hematite photoanodes. Reproduced from ref. 83 with permission from John Wiley and Sons, copyright 2017. (c) Space charge region (*W*) and charge carrier density (N_D) profile of nanoparticles. Reproduced from ref. 82 with permission from John Wiley and Sons, copyright 2020. (d) *I*–*V* curve analysis of unbranched nanorod (NR) and branched nanorod (BNR) Ti-doped hematite photoanodes. (e) Fabrication of porous Si:Ti–Fe_2O_3. Reprinted with permission from ref. 83, Copyright 2022 American Chemical Society.

hematite exhibits enhanced charge separation, as depicted in Fig. 9b. However controllable doping yields more effective results than unintentional doping (Fig. 9c).[95] Moreover, they explored the effects of Si doping, a semiconductor material which led to an overall improvement in performance. The analysis of the transient photocurrent density curve demonstrated a low recombination rate when Si is doped.[94]

Metal doping enhances the charge carrier's density, hence conductivity, however, it also has negative effects such as a high electron–hole recombination rate on the surface of hematite. To address the negative effects of M-doping (M–Sn and Ti), a cost-effective strategy of boron (B), a nonmetal, doping into metal-doped hematite has been employed and it improves the performance of PEC devices.[96] The secondary B-doping of broadly used M-doped hematite photoanodes not only suppresses the number of M^+ ions, which inevitably cause electron–hole pair recombination but also generates an internal electric field for easy hole extraction (Fig. 10a and b). The optimized M:B-Fe_2O_3 with a film thickness of 900 nm exhibited greatly reduced recombination and presented a photocurrent density of 1.92 mA cm^{-2} at 1.23 V_{RHE} and 2.83 mA cm^{-2} at 1.50 V_{RHE}. The strategy paves the way to reducing the recombination of electron–hole pairs of M-doped hematite and potentially improving the PEC water-splitting performance, which solves the length limitation issue of hematite. Nonmetal phosphorus (P) is also an excellent dopant that greatly improves the charge separation efficiency, and the fabrication of P-doped hematite electrodes typically involves techniques such as impregnation and hydrothermal methods.[97] These P-doped hematite electrodes exhibit a photocurrent density of 2.7 mA cm^{-2} at 1.23 V (*vs.* RHE) for water splitting, which was significantly higher than that of bare hematite (0.83 mA cm^{-2}). Moreover, the

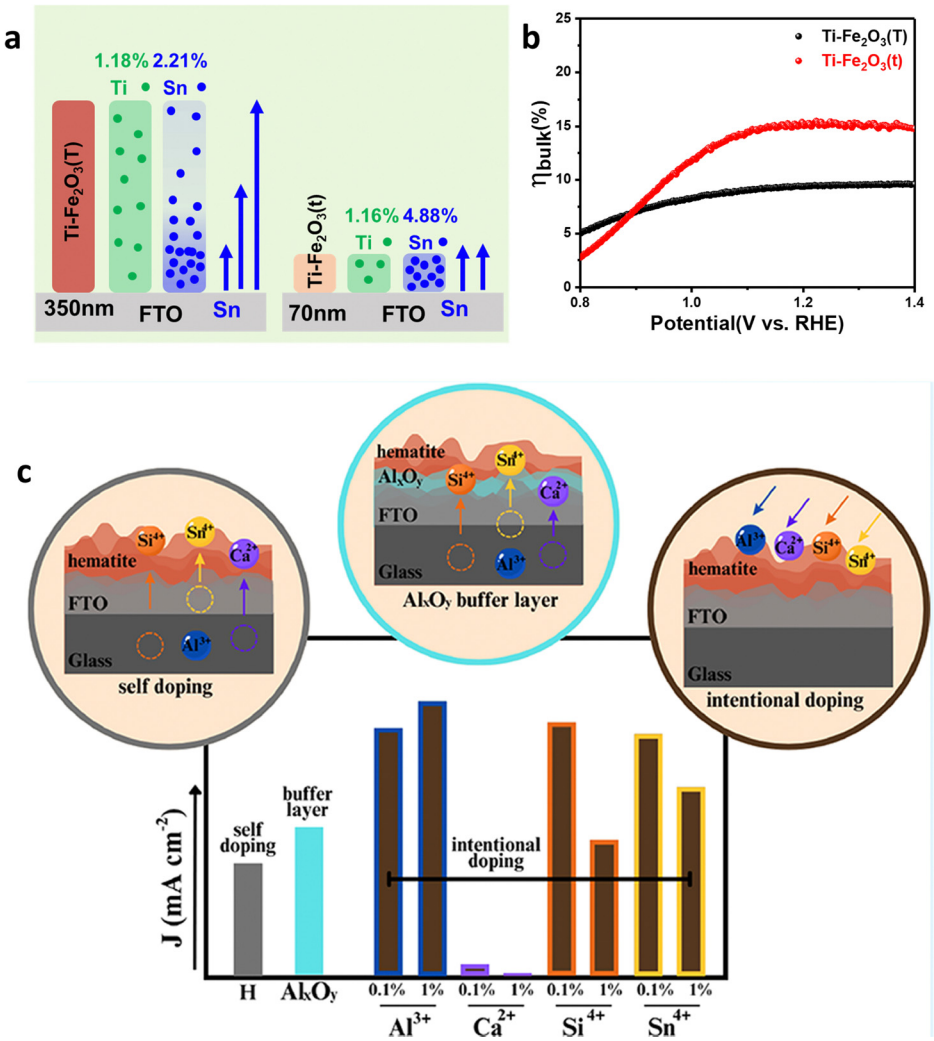

Fig. 9 Intentional and unintentional doping. (a) Distribution of Sn^{4+} and Ti^{4+} dopants in Ti–Fe_2O_3(T) and Ti–Fe_2O_3(t) systems. (b) Bulk charge separation efficiency (η_{bulk}) of Ti–Fe_2O_3(T) and Ti–Fe_2O_3(t). Reproduced from ref. 94 with permission from Elsevier, copyright 2020. (c) Difference between intentional and unintentional doping. Reprinted with permission from ref. 95, Copyright 2023 American Chemical Society.

introduction of phosphorus in hematite enhances the electron mobility. However, it should be noted that homogeneous doping can lead to a reduction in the width of the space charge region, which may be detrimental to effective charge separation. To mitigate this concern, a novel approach was employed to develop a gradient P-doped hematite nanoarray photoanode, which demonstrated remarkable performance in photoelectrochemical water oxidation. The researchers discovered that brief thermal treatment (10 minutes at 750 °C) of hematite after immersion in a phosphate solution facilitated the formation of a gradient P-doped structure. This incorporation of P was attributed to the diffusion of P from the surface towards the core of hematite during the thermal treatment, driven by the concentration disparity of P between the surface and the bulk. By ceasing the thermal treatment, the diffusion rate of P decreased, resulting in the formation of a gradient P-doped hematite nanoarray photoanode. However, prolonged thermal treatment (30 minutes at 750 °C) led to a reduction in the concentration gradient of P, eventually approaching homogeneous doping.[98]

The latest report on mesopore generating P-doped Ti-hematite shows excellent performance.[99] This study introduces a novel approach to fabricating P-doped hematite with mesopores and gradient doping properties using a cost-efficient *in situ* hydrothermal process. The P, Ti–Fe_2O_3 photoanode demonstrates a significantly improved PEC performance due to factors such as increased electrical conductivity through oxygen vacancies, reduced hole diffusion path length, enhanced charge separation *via* non-metal P doping and steeper band bending achieved by reducing the depletion region (DR) (Fig. 10c). Additionally, the P,Ti–Fe_2O_3 photoanode exhibits enhanced stability for 20 hours, highlighting the practical utility of P doping in PEC systems. The application of a co-catalyst, $NiFeO_x$, further enhances the photocurrent density (3.54 mA cm^{-2} at 1.23 V_{RHE}) with a 108 mV cathodic shift.

While doping, formation energy, and crystal disorder play an important role. Research by Yoon *et al.*[87] explore nonmetal Si doping in hematite using a Ti dopant to improve its performance as a photoelectrode for water splitting. The study

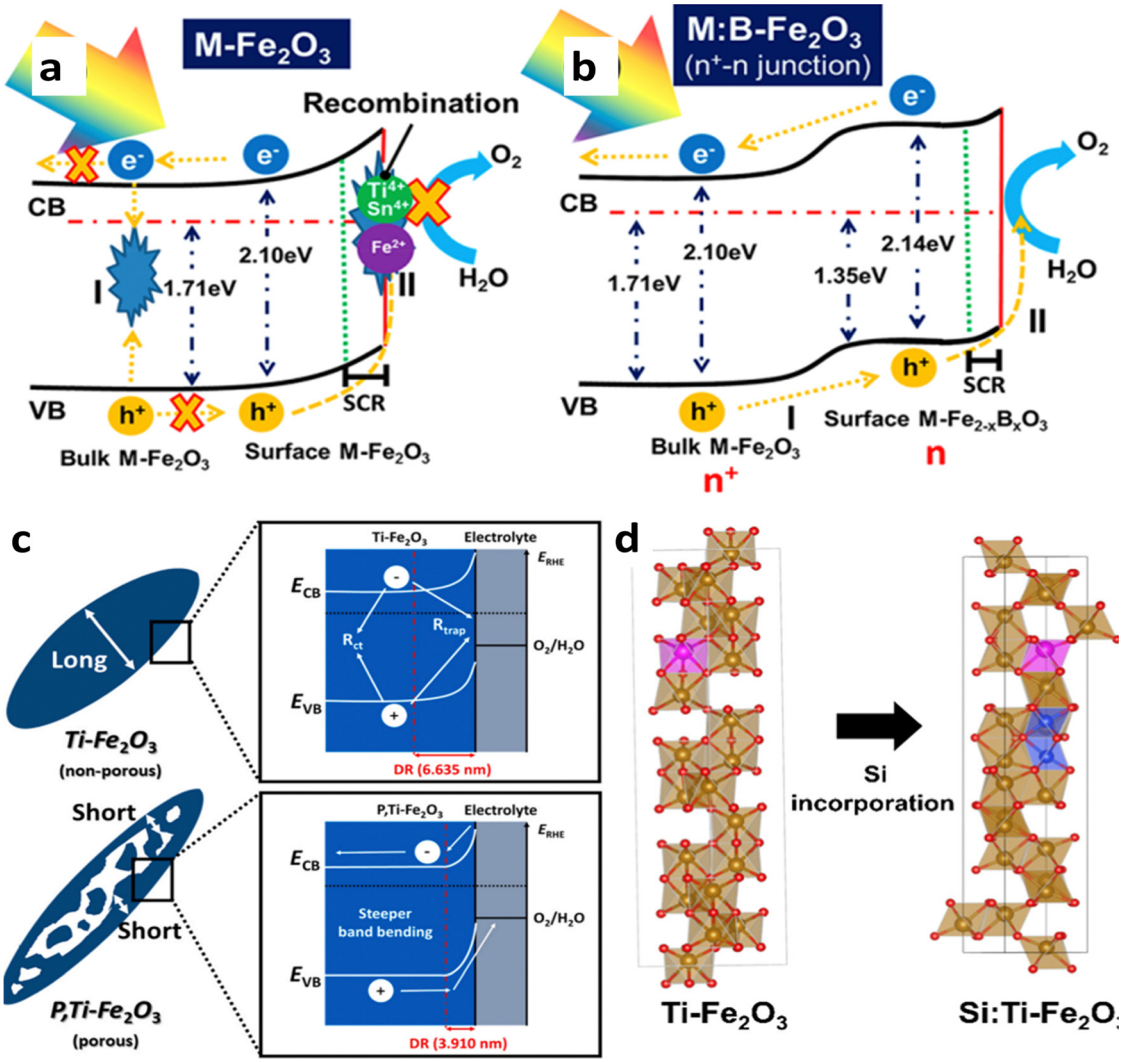

Fig. 10 Impact of nonmetal and favorable doping. (a) Charge transfer process in metal-doped, and (b) M:B-doped hematite. Reprinted with permission from ref. 96, Copyright 2023 American Chemical Society. (c) Mechanism behind the high performance of Ti and P co-doped hematite. Reproduced from ref. 99 with permission from Elsevier, copyright 2022. (d) Mitigation of disordered regions by favorable Ti doping. Reprinted with permission from ref. 87, Copyright 2022 American Chemical Society.

demonstrates a cost-efficient solution-based method for Si doping and achieves a high photocurrent density of 4.3 mA cm^{-2}. The results highlight the importance of formation energy and crystal disorder in doping feasibility and PEC activity. They find that the formation energy of unfavorable dopant (Si) can be reduced by favorable doping (Ti) and the crystal disorder caused by unfavorable dopant Si can be minimized by favorable doping with Ti (Fig. 10d). The approach also offers a simpler and more cost-effective alternative to current doping methods and shows potential for improving PEC performance in other systems.

Besides elemental doping, molecular doping, and multi-elemental doping are also well-known strategies to improve the charge separation efficiency.[100–102]

5.1.3. Junction. The formation of a junction is a promising approach to improve charge separation within the semiconductor bulk. These junctions can take the form of metal–semiconductor (Schottky) junctions or semiconductor–semiconductor junctions. By inducing or enhancing the built-in field, these junctions deepen the depletion of electrons (holes) in the hematite material, resulting in decreased electron affinity and increased work function.

Chen *et al.*[103] fabricated a Ti/Au/Fe_2O_3 photoanode structure, where Au nanoparticles (NPs) were present both above and below the hematite layer. The junction formed between Au NPs and hematite improved the charge separation efficiency by acting as electron collectors at the hematite–fluorine doped tin oxide substrate interface (Fig. 11a). Similar results have been reported by other researchers.[104] When a small amount of Au NPs was loaded onto the hematite electrode, an Au–semiconductor contact (Schottky contact) was formed, leading to Fermi-level equilibration and improved charge transport efficiency.

Besides metal–semiconductor junctions, semiconductor–semiconductor (S–S) junctions are also employed to enhance charge separation. S–S junctions can be classified as

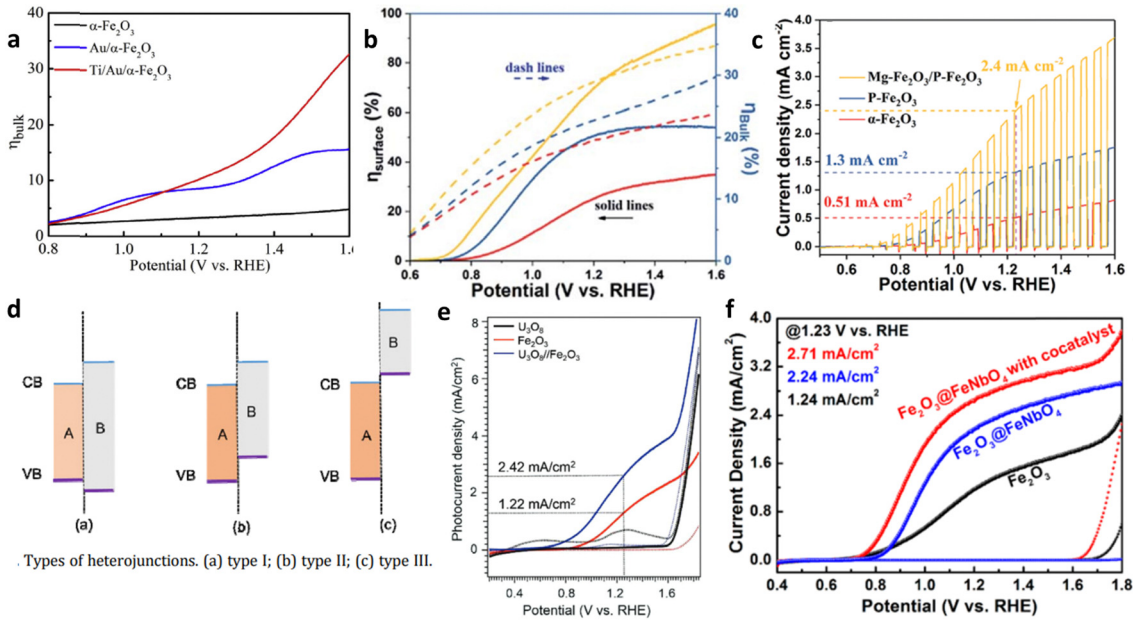

Fig. 11 Homo- and hetero-junctions of hematite. (a) Effect of a Schottky junction on the bulk charge efficiency of hematite-based anodes. Reproduced from ref. 103 with permission from Elsevier, copyright 2018. (b) Surface and bulk charge efficiency of homojunction based hematite photoanodes. (c) Transient current density analysis of homojunction based hematite photoanodes. Reproduced from ref. 105 with permission from Royal Society of Chemistry. (d) Classification of heterojunctions. (e) Reproduced from ref. 108 with permission from John Wiley and Sons, copyright 2019. (f) *J*–*V* curve analysis of heterojunction-based hematite electrodes. Reprinted with permission from ref. 109, Copyright 2019 American Chemical Society.

homojunctions or heterojunctions. Ma *et al.*[105] fabricated a photoanode composed of Mg-doped and P-doped hematite nanorods, demonstrating high charge separation capacity (Fig. 11b and c). Improved conductivity and favorable charge separation efficiency resulted from the built-in electric field, as revealed by experimental and density functional theory analyses.

S–S heterojunctions are further categorized into three types based on the relative positions of the conduction band and valence band between the semiconductors (Fig. 11d). Among these types, only type II heterojunctions, which is a staggered alignment, enable efficient charge separation in all dimensions because the conduction band minimum of one semiconductor is below that of the other semiconductor, and the valence band maximum of the first semiconductor is above that of the second semiconductor. This band alignment creates a built-in electric field that promotes the separation and transport of carriers.[106,107] For instance, a U_3O_8/Fe_2O_3 heterojunction photoanode exhibited enhanced PEC performance compared to the bare Fe_2O_3 photoanode.[108] The U_3O_8/Fe_2O_3 system showed type II band alignment, facilitating faster-photoinduced electron injection and strengthened charge carrier separation, which leads to an overall high performance (Fig. 11e)

Additionally, core–shell heterojunction photoanodes were synthesized using hybrid microwave annealing.[109] Fe_2O_3 nanorods served as the core, while $FeNbO_4$ thin layers formed the shell. The Fe_2O_3@$FeNbO_4$ electrode displayed higher water oxidation activity compared to the bare Fe_2O_3 electrode, due to an improved bulk and surface separation efficiency (Fig. 11f). This superior PEC performance was attributed to the band alignment, which promoted efficient charge separation.

5.1.4. Oxygen vacancy. Recent investigations have focused on the impact of oxygen plasma treatment on hematite photoanodes (because the prepared hematite faces oxygen deficiency problems[110]), revealing noteworthy effects on their performance. Two studies conducted by Hu *et al.*[110] and Pyeon *et al.*[111] demonstrate that such treatment results in increased photocurrent densities, albeit with a higher onset potential. X-ray photoelectron spectroscopy analysis conducted by Hu *et al.* reveals a reduction in the concentration of surface Fe^{2+} species accompanied by an increase in OH^- species. Pyeon *et al.* corroborated these findings and further demonstrated that a subsequent short annealing step not only recovers the photocurrent but also enhances it (Fig. 12a). This phenomenon is attributed to the oxygen plasma treatment filling oxygen vacancies and attracting additional OH^- species due to the increased oxidation state of Fe (Fig. 12b). Following the short annealing, newly formed oxygen vacancies are brought closer to the surface (Fig. 12c). Given that both oxygen vacancies and the density of charge transfer band and upper hubber band have a direct influence on the photocurrent curves, these findings offer valuable insights into optimizing hematite photoanode performance.

5.1.5. Conclusion. Issues such as short carrier lifetime, limited mobility, and restricted diffusion length limit reaching the theoretical photocurrent of hematite (12.6 mA cm^{-2} under 600 nm). The bulk charge separation efficiency improves through nanostructuring, doping, junction formation, and the introduction of oxygen vacancy. Nanostructuring and doping show promise, as particle size decreases, enhancing photocatalytic activity. Tailoring structures, such as creating nano wire-type configurations, aligns with charge diffusion lengths,

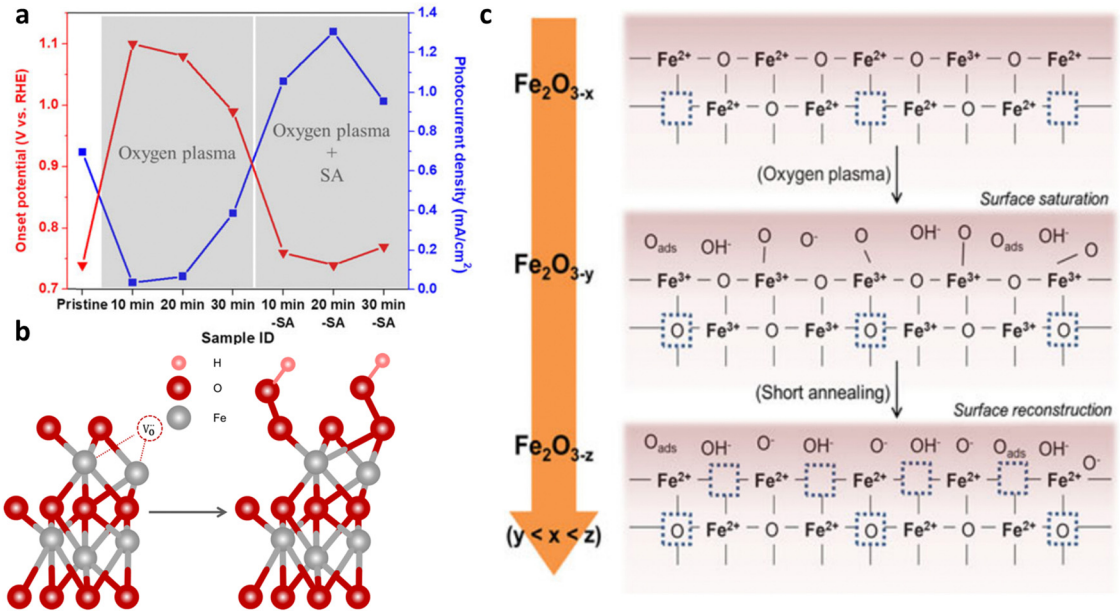

Fig. 12 Impact of oxygen plasma treatment. (a) Plasma treatment effects, with and without short annealing, on the onset potential and photocurrent density at 1.23 V_{RHE}. (b) Formation of FeOOH on the (0001) surface of hematite as a result of oxygen plasma treatment. Reprinted with permission from ref. 110, Copyright 2016 American Chemical Society. (c) Effect of post-treatment on the hematite surface. Reproduced from ref. 111 with permission from Springer Nature, copyright 2018.

while smaller particle sizes increase charge carrier densities. Fabricating photoanodes with high transfer capabilities and absorption efficiencies, achieved through small particle branching, enhances charge separation. Establishing junctions improves bulk charge separation, and incorporating oxygen vacancies enhances PEC performance.

5.2. Interfacial charge separation modification

The interface between the substrate–hematite and hematite–cocatalyst behaves as a recombination center. Other than these two interfaces, grain boundaries also cause severe recombination of electrons–holes, which leads to an overall low internal quantum efficiency.

5.2.1. Modification of the substrate–hematite interface. Utilizing a machine learning-based prediction model, it has been suggested that interfacial resistance stands out as a pivotal factor for enhancing charge separation, consequently influencing overall performance. The introduction of a TiO_2 underlayer not only improved the electrical properties at the interface but also enhanced the overall quality of hematite films (Fig. 13a and b).[112] The introduction of a TiO_2 underlayer beneath hematite in the study conducted by Luo *et al.*[83] effectively addressed the issue of interfacial recombination between the substrate (*e.g.* FTO) and hematite. Similar (underlayer-overlayer deposition of TiO_2) studies have also been carried out by many research groups.[113–115] This approach not only improves the PEC performance but also alleviates the recombination effects resulting from the lattice mismatch between the substrate and hematite by creating a type-II heterojunction.[116] The study by Luo *et al.* presents a novel approach to enhance the PEC water oxidation performance of hematite nanoarrays. By incorporating an ultrathin TiO_2 interlayer and an iron oxide hydroxide (FeOOH) cocatalyst, significant improvements in photocurrent and charge separation are achieved. The TiO_2 interlayer acts as a passivation layer and dopant source, reducing substrate/hematite charge recombination and increasing electrical conductivity. Additionally, the introduction of three-dimensional hierarchical branches on the hematite nanoarrays increases the surface area for improved charge collection (Fig. 13c). The FeOOH cocatalyst further enhances PEC performance by accelerating the oxygen evolution reaction.[115,117,118] The optimized photoanode exhibits a photocurrent density of approximately 3.1 mA cm^{-2} at 1.23 V (*vs.* RHE), surpassing previous Ti-doped hematite photoanodes (Fig. 13d).

5.2.2. Modification of the cocatalyst–hematite interface. The interface between the oxygen-evolution catalysts (OECs) and photoelectrodes leads to a drawback related to the transfer of charges. This issue arises due to suboptimal interactions between the catalyst and the electrode interface, resulting in inadequate contact and detachment of the catalysts from the electrode substrate.[119] Park *et al.*[120] decorated the nano-fragmented 0D MXene (NFMX) between hematite and OEC ($NiFe(OH)_x$) as a hole transport layer (Fig. 14a) so that the potential of the OEC can be fully utilized. Leveraging its high reactivity, efficient hole extraction, and transport capabilities, NFMX proves to be an excellent hole transport material. However, the coating lacks uniformity, as shown in Fig. 14a, which somewhat reduces the potential of the OEC and results in a current density of 3.09 mA cm^{-2}. To mitigate this Ahn *et al.*[121] investigated the potential of using siloxane-modified diketopyrrolopyrrole (DPP)-based π-conjugated (P_{Si}) organic semiconductors (OSs) as a hole transport layer between

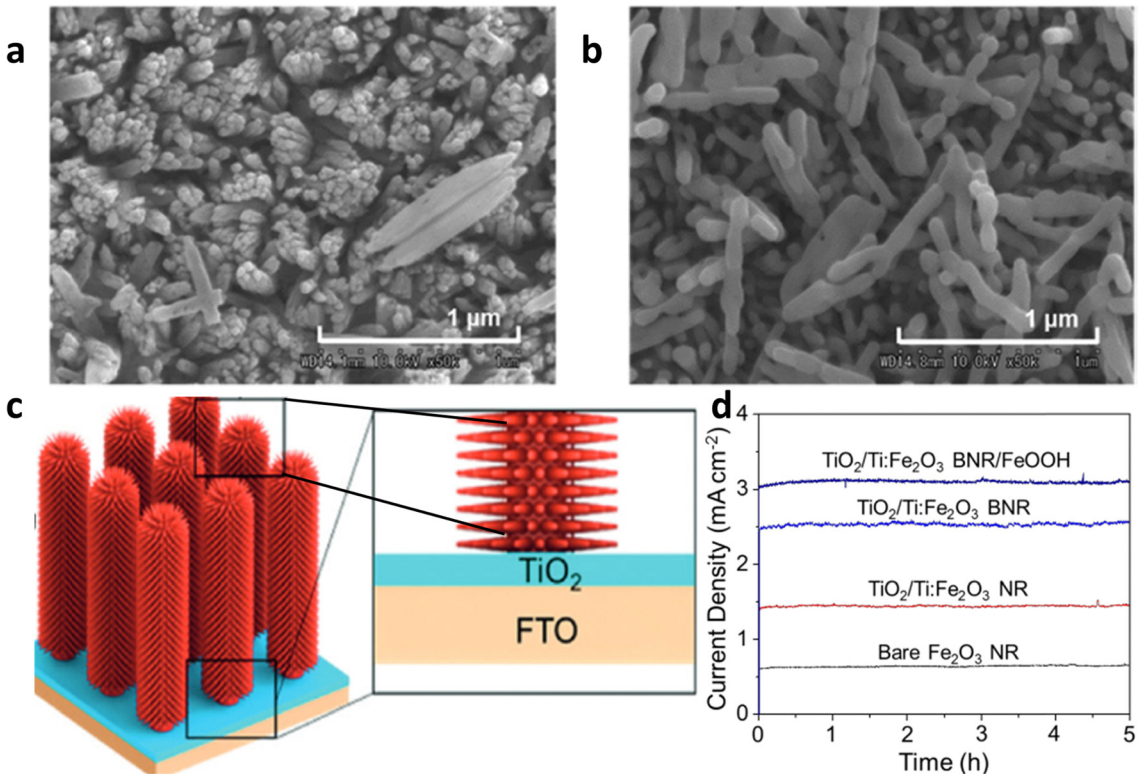

Fig. 13 Impact of underlayer TiO_2. (a) Hematite grown on FTO. (b) Hematite grown on TiO_2-coated FTO. Reprinted with permission from ref. 112, Copyright 2023 American Chemical Society. (c) Decoration of the TiO_2 layer between the branched hematite nanorod photoanode and FTO substrate for the synthesis of BNR. (d) Stability curve of the bare nanorod hematite photo anode with or without a branch, TiO_2 modification layer, and the cocatalyst. Reproduced from ref. 83 with permission from John Wiley and Sons, copyright 2017.

hematite photoanodes and OECs for efficient photoelectrochemical water splitting. The results demonstrate that incorporating the P_{Si} OS (Fig. 14b) with high crystallinity enhances the stability of the photoanode in water and significantly improves its charge separation efficiency (Fig. 14c). The NiFe-$(OH)_x$/P_{Si}/Ge-PH photoanode exhibits a high photocurrent density of 4.57 mA cm^{-2} (Fig. 14d) and excellent stability over a prolonged period (>60 h). The study suggests a simple yet effective approach to enhance charge extraction and transfer by achieving conformal contact between the OS layer and the hematite photoanode. Additionally, the combination of organic and inorganic semiconductors forms a type-II heterojunction, promoting efficient hole extraction. The investigation also includes calculations of bulk and surface charge separation efficiencies, which confirm the benefits of the heterojunction for rapid charge separation.

5.2.3. Grain boundary modification of hematite. Furthermore, the grain boundaries in hematite have been identified as charge-blocking components,[122,123] serving as recombination centers. Feng *et al.*[124] introduced an effective approach to enhance charge separation by decorating the grain boundaries of hematite with TiO_2 (Fig. 15a). This work presents an efficient strategy for enhancing charge transfer in hematite photoanodes by decorating the grain boundaries (Fig. 15b and c) with TiO_2 using a simple chemical bath deposition method. The incorporation of TiO_2 at the grain boundaries results in a significant improvement in photocurrent density, reaching 2.90 mA cm^{-2} at 1.23 V *vs.* RHE. The IPCE and APCE values also show substantial increases, reaching 68% and 95% at 360 nm, respectively. The enhanced charge separation efficiency, increased charge carrier density, and enlarged contact area between the electrolyte and the photoanode contribute to the superior photoelectrochemical performance of the TiO_2-decorated hematite film. Furthermore, the addition of FeOOH catalysts to the modified film leads to even higher photocurrents, achieving 3.15 mA cm^{-2} at 1.23 V *vs.* RHE. Another new and more effective strategy, introduced by Pires *et al.*[125] involves the selective placement of modifiers. Here, they present a novel approach using a single polymeric precursor solution for the design of α-Fe_2O_3 with synergistic bulk and interfacial engineering involving Ga^{3+}, Hf^{4+}, and $NiFeO_x$. The solution induces Ga^{3+} doping to alleviate polaronic effects, enriches Hf^{4+} at surface and grain boundaries for enhanced charge separation, and promotes a refined microstructure through interface stabilization. Combined with Ga^{3+} bulk doping and $NiFeO_x$ electrodeposition, the modified hematite photoanode (176 nm-thick) achieves an overall photoelectrode efficiency of 65%, yielding a significantly improved water oxidation photocurrent of 2.30 mA cm^{-2} at 1.23 V_{RHE} compared to 0.37 mA cm^{-2} for the pristine system (Fig. 15d).

5.2.4. Conclusion. Optimizing interfacial resistance is crucial for enhancing charge separation in PEC photoanodes. Three key interfaces deserve attention: hematite–substrate (usually FTO), hematite–catalysts, and hematite grain boundaries. Grain

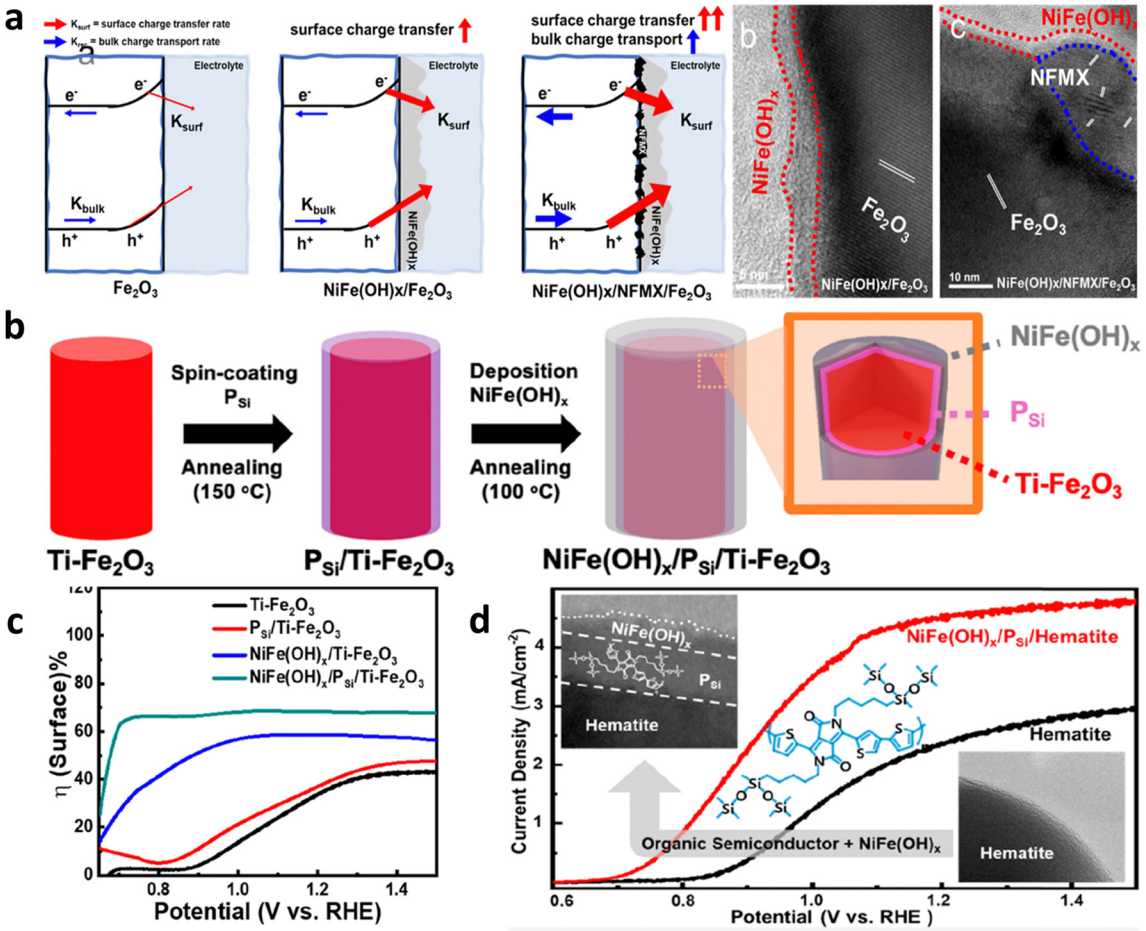

Fig. 14 Conformal contact between the co-catalyst and hematite. (a) Role and TEM image of NFMX decorated hematite. Reprinted with permission from ref. 120, Copyright 2023 American Chemical Society. (b) Decoration of an organic semiconductor (OS) at the interface between hematite and the co-catalyst. (c) Improvements in surface charge transfer efficiency due to organic semiconductor incorporation. (d) Performance curve of the OS-incorporated hematite photoanode. Reprinted with permission from ref. 121, Copyright 2023 American Chemical Society.

boundary modifications, along with the other interfaces, impact charge separation efficiency significantly. For instance, introducing a TiO_2 underlayer between FTO and hematite mitigates recombination and lattice mismatch, by forming type-II heterojunctions and also promoting uniform hematite growth. Overlayers such as organic semiconductors and MXenes between hematite and co-catalysts enhance charge separation through type-II junctions and act as hole extractors. Both underlayer and overlayer modifications show potential for improving charge separation efficiency. Crucially, grain boundary modifications significantly enhance surface and bulk charge separation, contributing significantly to overall PEC photoanode performance. Current research trends include simultaneous multi-elemental doping, selectively improving polaronic effects, grain boundaries, surface states, and other relevant factors.

5.3. Modification of surface charge separation efficiency

There are three primary processes that take place on the surface of the photoanode: recombination of carriers, water oxidation, and back reactions. Consequently, enhancing the surface charge efficiency can be achieved through three key approaches: minimizing surface recombination, enhancing the kinetics of the water oxidation reaction, and mitigating the occurrence of back reactions.

5.3.1. Passivation of surface states. The migration of holes from the bulk to the surface of hematite often results in significant recombination.[126] In the case of semiconductors, two important effects should be considered: the potential drop across the space charge layer and the Helmholtz layer at the interface between the semiconductor and the solution (excluding the diffusion layer in the solution). Due to the considerably higher capacitance of the Helmholtz layer compared to the space charge layer capacitance, the primary potential drop occurs in the space charge layer, while the Helmholtz potential remains constant. This leads to a nearly unchanged position of the semiconductor's band edge (band edge pinning effect).[127] Under conditions of band edge pinning, an increased applied potential induces band bending, which facilitates the separation of carriers generated by light. However, the presence of surface states causes the relative positions of the Fermi level and the surface band edge to remain fixed, resulting in unchanged band bending even with variations in the applied potential (Fermi level pinning effect).[127] This

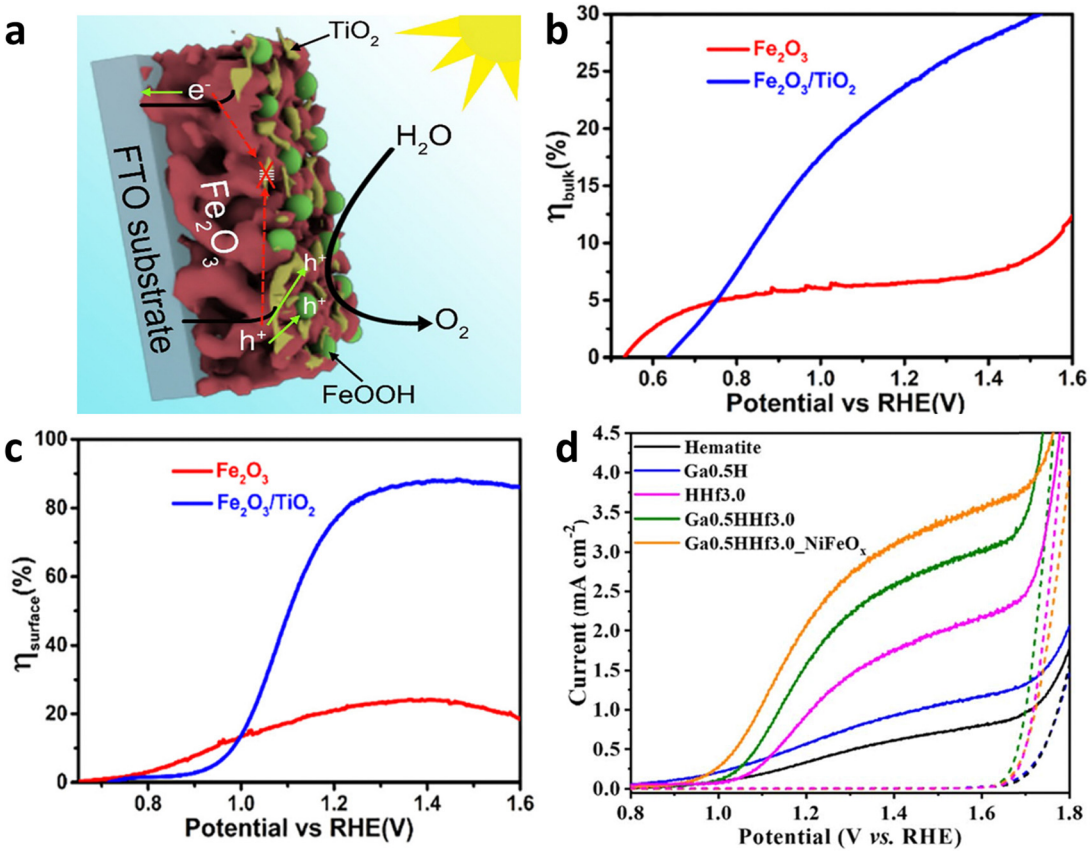

Fig. 15 Grain boundary modification by metal oxide and elemental doping. (a) Decoration of TiO_2 on grain boundaries. (b) and (c) Surface and bulk charge efficiency improvement by grain boundaries modification. Reproduced from ref. 124 with permission from Elsevier, copyright 2019. (d) *J*–*V* curve analysis of grain boundaries modified hematite photoanodes. Reproduced from ref. 125 with permission from Royal Society of Chemistry, copyright 2023.

phenomenon has an impact on the separation of carriers generated by light. Therefore, the reduction of surface recombination can be achieved by passivating surface states. Additionally, surface recombination can be mitigated by reducing the electron density on the semiconductor surface[128] and by the regrowth mechanism (by reducing surface disorder).[129] The surface state of hematite can be modified by intrinsic engineering or by extrinsic engineering. Intrinsic modifications including sintering,[130] acid treatment,[131] and regrowth mechanism[132] could improve the charge transfer by suppressing surface state recombination.

Sintering. The sintering parameters, which encompass temperature, duration, and atmosphere, play a crucial role in enhancing the photoelectrochemical performance of hematite-based photoanodes by reducing crystal defects. It has been reported that controlling the sintering temperature not only facilitates the diffusion of Sn from FTO into the hematite matrix but also modifies the surface states present on the photoanode's surface.[133] A study by Zandi *et al.*[134] demonstrated that annealing hematite at 800 °C significantly enhances the water oxidation efficiency of ultrathin film hematite electrodes. This improvement is attributed to the elimination of surface states in close proximity to the conductance band of the hematite photoanodes, leading to a reduction in recombination and Fermi-level pinning (Fig. 16a and b). The presence of two surface states (two peaks) at 500 °C and their elimination with a cathodic shift at 800 °C can be seen in Fig. 16c. Similarly, the work by Si *et al.*[135] reveals a simple yet effective protonation-annealing treatment to mitigate both bulk and surface charge recombination in hematite. Electrochemical incorporation of protons/electrons at 0.2 V_{RHE}, followed by annealing at 120 °C, significantly enhances the photocurrent density from ~0.9 to 2.7 mA cm^{-2} at 1.23 V_{RHE} under 1 sun illumination (Fig. 16d). The introduction of cobalt phosphate further stabilizes the performance around 2.4 mA cm^{-2} (Fig. 16e). Unlike prior attributions to the formation of Fe_3O_4 or metal Fe, this work emphasizes that the improvement is primarily linked to proton incorporation. Repeated treatments cathodically shift the onset potential, increase donor density, and reduce bulk recombination, while low-temperature annealing minimizes surface recombination (due to the lowest charge transfer resistance (Fig. 16f)), maintaining high bulk charge separation efficiency.

Acid or alkaline treatment. Another intrinsic method is the surface treatments using acidic or alkaline media, which have been investigated as a means to modify the surface states of hematite electrodes, resulting in improved photoelectrochemical

water-splitting performance through enhanced charge separation efficiency.[136–138] Li *et al.*[139] conducted a study to examine the impact of acidic media (including acetic acid, HCl, HNO_3, and H_3PO_4) treatment on hematite photoanodes. They demonstrated that a simple acid treatment method can modify the nature or position of available trap sites, leading to a significant enhancement in the efficiency of electron movement out of traps in hematite nanowire photoanodes. This is because of the reduction in charge transfer resistance (Fig. 17a). Consequently, this reduces electron–hole recombination losses and improves the overall PEC performance (Fig. 17b). However prolonged acid treatment could cause lattice defects, which will serve as recombination centers. A study by Wang *et al.*[140] revealed the impact of HCl treatment on Ti-, Ge-, Pt-, and Sn-doped photoanodes, as summarized in Fig. 17c. The *ex situ* doping method results in a significant dopant distribution across the surface. With an appropriate treatment time (1 h), a portion of the surface Fe–O bonds is removed, leading to an increase in M–O bonds that passivate surface states and enhance hole transfer. The promoting effect is most pronounced for Ti–O among the Ti, Ge, Pt, and Sn dopants. Consequently, HCl treatment significantly improves the performance of Ti, TiGe, TiPt, and TiSn photoanodes. However, prolonged HCl treatment (2 h) leads to further corrosion of near-surface Fe–O bonds, creating excess lattice defects that can act as electron/hole recombination centers. In summary, HCl serves a dual role in *ex situ*-doped α-Fe_2O_3: it alters surface elemental components and forms lattice defects. Similarly, Ye *et al.*[141] observed a threefold and twofold increase in photocurrent densities for α-Fe_2O_3 and Ti:α-Fe_2O_3 photoanodes, respectively, after treatment with KOH. They attributed this improvement to the formation of a conformal thin layer on the hematite surface, grafted with hydroxyl (–OH) groups, which acts as an electrocatalyst, accelerating the water oxidation kinetics on the hematite photoanodes.

A general extrinsic technique for surface passivation and reduction of surface recombination involves the application of a thin passivation layer on the surface of hematite.[142–144] Bahnemann *et al.*[145] conducted a study where they achieved surface passivation by coating a hematite electrode with a layer of TiO_2. The TiO_2 layer was deposited using a simple dipping-annealing process, resulting in an estimated thickness of less than 2 nm. The performance of photoelectrochemical water splitting was evaluated and depicted in Fig. 18a. The results revealed a significant enhancement of nearly 3.5-fold in the photocurrent due to the TiO_2 coating. Prior to the TiO_2 coating, the photovoltage was low (0.26 V) due to Fermi-level pinning. However, after the TiO_2 coating, the photovoltage increased to 0.46 V (Fig. 18b). The authors concluded that the coating enhanced the photovoltage by suppressing surface states. A similar study was carried out by Zhou *et al.*;[146] they decorated the Al_2O_3 underlayer and overlayer and conducted a comparative study. Their research found that Al_2O_3 deposition reduces the charge transfer resistance, thereby increasing the performance of hematite photoanode. Another strategy involves coating photoactive compounds; for example, Zhu *et al.*[147] coated L-cysteine (L-(C)ys) on porous hematite to passivate the surface state, providing an alternative route for water oxidation and lowering the charge transfer. The strong complexation

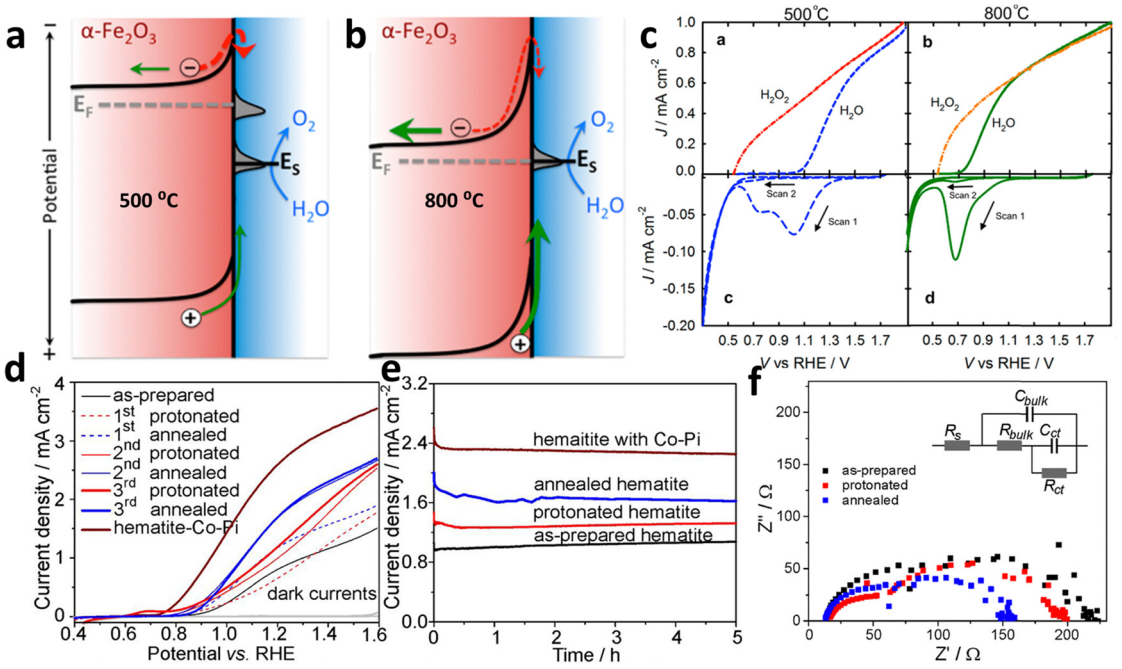

Fig. 16 Modification of surface state *via* annealing. (a) Upon heating at 500 °C, two surface states can be seen. (b) Upon heating at 800 °C, there is one surface state missing. (c) Cathodic shift in the cyclic voltammetry upon heating at 800 °C can be observed. Reprinted with permission from ref. 134, Copyright 2014 American Chemical Society. (d) Performance curve of the protonated-annealed hematite. (e) Stabilization test of annealed hematite. (f) Charge transfer resistance analysis by EIS. Reprinted with permission from ref. 135, Copyright 2014 American Chemical Society.

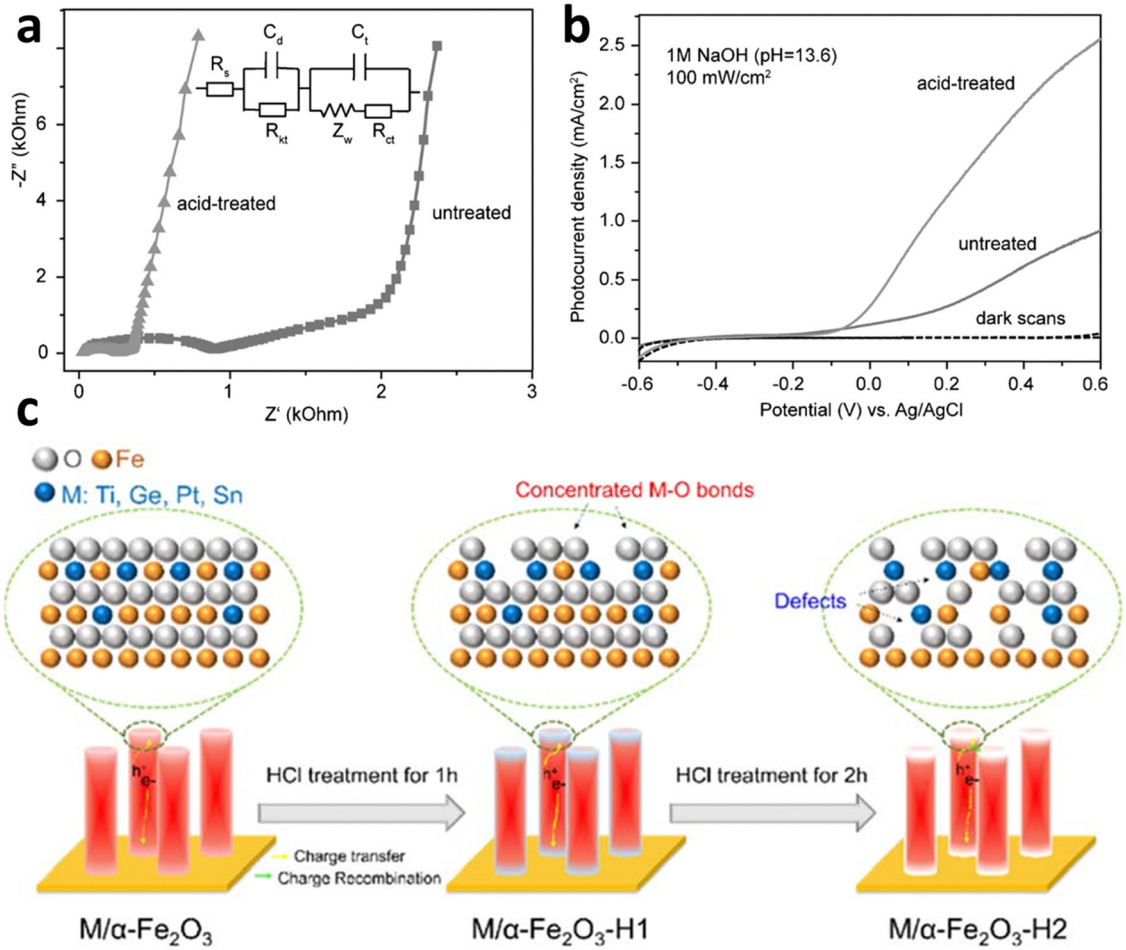

Fig. 17 Surface modification by acid. (a) EIS data shows acid treatment reduces the charge transfer resistance due to the passivation of surface states. (b) Effect of acid treatments (dil. HCl) on PEC performance. Reproduced from ref. 139 with permission from John Wiley and Sons, copyright 2016 (c). Effect of HCl treatment on doped hematite photoanode. Reproduced from ref. 140 with permission from Royal Society of Chemistry, copyright 2023.

interaction between hematite and (L)-Cys enables direct photo-oxidation, generating additional electrons for efficient H_2 production (Fig. 18c). The Ti-doped porous hematite (Ti-PH) photoanode achieves a current density of up to 4.45 mA cm^{-2} at 1.23 V *vs.* RHE under AM1.5 G illumination.

5.3.2. Accelerating the water oxidation reaction. Along with optimizing the intrinsic characteristics of hematite material, the integration of an OER catalyst onto the hematite surface represents a promising strategy to enhance hole injection efficiency.[148–150] It is important to highlight that the application of an inorganic catalyst layer on the hematite surface can fulfill multiple functions, including the mitigation of electron–hole recombination and the acceleration of OER kinetics.[151] A comparative study of molecular catalyst (Ir) (het-WOC) and metal oxide catalysts (IrO_x) on hematite for PEC water oxidation has been performed by Wang *et al.*[152] They found that the het-WOC catalyst, when applied as a thin layer on the hematite photoanode, significantly improved the system's performance by enhancing charge transfer by 42-fold (Fig. 19a). Importantly, this improvement occurred without changing the surface recombination rate (Fig. 19b).

In contrast, in a comparative study (Fig. 20a–c), the IrO_x catalysts improved the PEC performance by reducing the surface recombination rate, effectively replacing the original $Fe_2O_3|H_2O$ interface with a different interface involving IrO_x (Fig. 20c). This resulted in faster charge transfer as well. The study suggests that the het-WOC catalyst provides additional charge-transfer pathways across the $Fe_2O_3|H_2O$ interface (Fig. 20b), while IrO_x and similar bulk metal-oxide catalysts create a fundamentally different interface (Fig. 20c).

Another strategy is to decorate doped metal oxides on the surface of a hematite-based photoanode. Jang *et al.*[153] developed an efficient water-splitting PEC cell by using a Ti-doped FeOOH co-catalyst on a Ti-doped porous hematite structure coated with a thin layer of SiO_x (the SiO_x layer facilitates charge extraction). The SiO_x layer enabled the preferential deposition of the Ti-FeOOH co-catalyst within the inner pores of the hematite, improving the performance of the oxygen evolution reaction without hindering light absorption by the hematite (Fig. 21a). The Ti-FeOOH/Ti-PH photoanode exhibited a high photocurrent density of 4.06 mA cm^{-2} at 1.23 V *vs.* RHE, which was 3.4 times greater than that of conventional worm-like

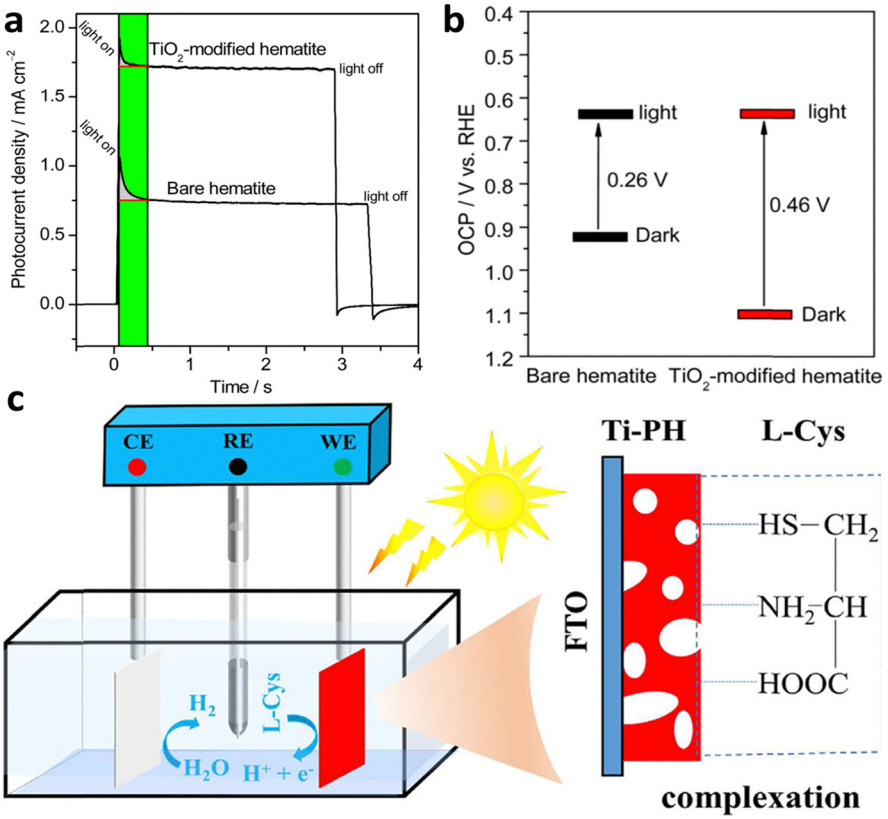

Fig. 18 Overlayer modification. (a) Transient current analysis of the hematite photoanode with or without TiO_2 coating. (b) Open circuit potential measurements under dark and illuminated conditions (photovoltage). TiO_2 coating enhances photovoltage by suppressing the surface state. Reprinted with permission from ref. 145, Copyright 2015 American Chemical Society. (c) L-cysteine grafted Ti-doped porous hematite (Ti-PH). Reproduced from ref. 147 with permission from Elsevier, copyright 2023.

hematite (Fig. 21b). Furthermore, it demonstrated excellent long-term stability for 36 hours. Another category of co-catalysis is single-atom catalysis,[154,155] and a study by Guo *et al.*[156] explored the role of single-atom iridium (sIr) catalysts on hematite photoanodes in the water-splitting mechanism. The results revealed that α-Fe_2O_3/sIr photoanodes act as true catalysts by capturing holes from hematite and facilitating water oxidation. Spectroscopic experiments showed reduced hole concentration and shortened lifetime in the presence of sIr, indicating faster hole transfer and depletion. Theoretical calculations demonstrated that sIr exhibited a lower energy barrier for water oxidation compared to iron sites (Fig. 21c).

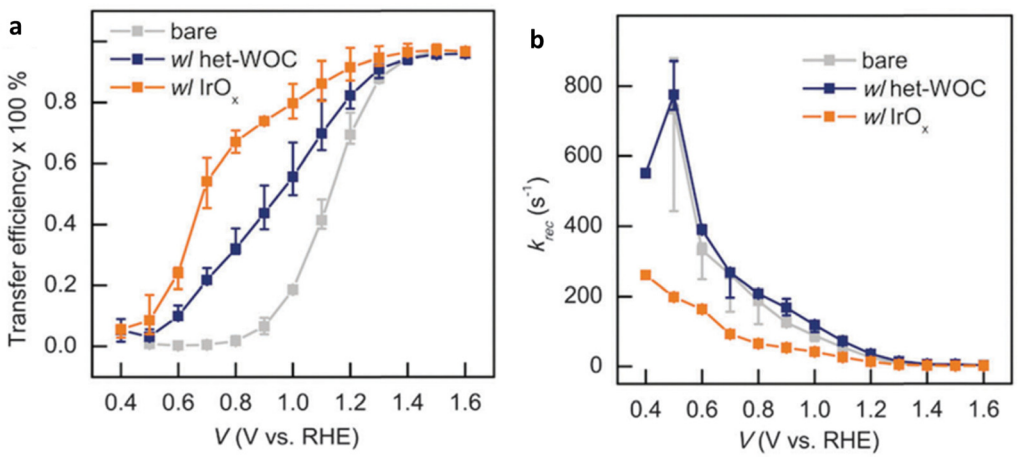

Fig. 19 Impact of heterogeneous catalysts (a). Transfer rate constant (K_{trans}) (b). Recombination rate constant (K_{rec}). Reproduced from ref. 152 with permission from Royal Society of Chemistry, copyright 2023.

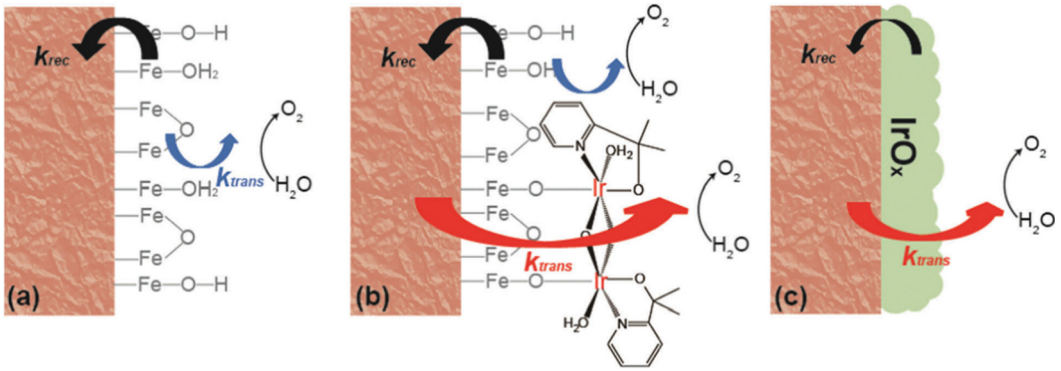

Fig. 20 Kinetic pathway for (a) hematite, (b) hematite with a molecular catalyst, and (c) hematite with a metal oxide catalyst. Reproduced from ref. 152 with permission from Royal Society of Chemistry, copyright 2023.

This study provides valuable insights into the interplay between electronic structure and hole transfer, highlighting the potential of single-atom cocatalysts for enhancing photoanode performance. However, S. Pokrantetal *et al.*[157] emphasized that in the realm of photocatalysis, the size distribution of a cocatalyst carries greater significance than the choice of a specific material. They noted that when it comes to photocatalysis, a preference exists for a smaller size distribution due to the electrokinetic effect. However, for photoelectrochemical cells, a larger particle size distribution is favored to mitigate the risk of high recombination rates.

5.3.3. Suppressing the back reaction. To improve the efficiency of hole injection in hematite photoanodes, it is important to minimize the back reactions associated with the OER kinetics. One effective strategy is the incorporation of a blocking layer. In certain cases where the hematite film on the substrate is incomplete, there can be a substrate–solution interface, allowing electrons from the substrate to react with intermediates or products (*e.g.*, O_2), thereby reducing hole utilization (Fig. 22a). However, the introduction of a blocking layer between the hematite film and the substrate significantly reduces the substrate–solution interface, effectively suppressing the back reactions.[158] Bouhjar *et al.*[159] utilized a thin hematite layer, electrodeposited as a blocking layer, on the underlying hematite material (Fig. 22b). This innovative approach resulted in outstanding photoelectrochemical

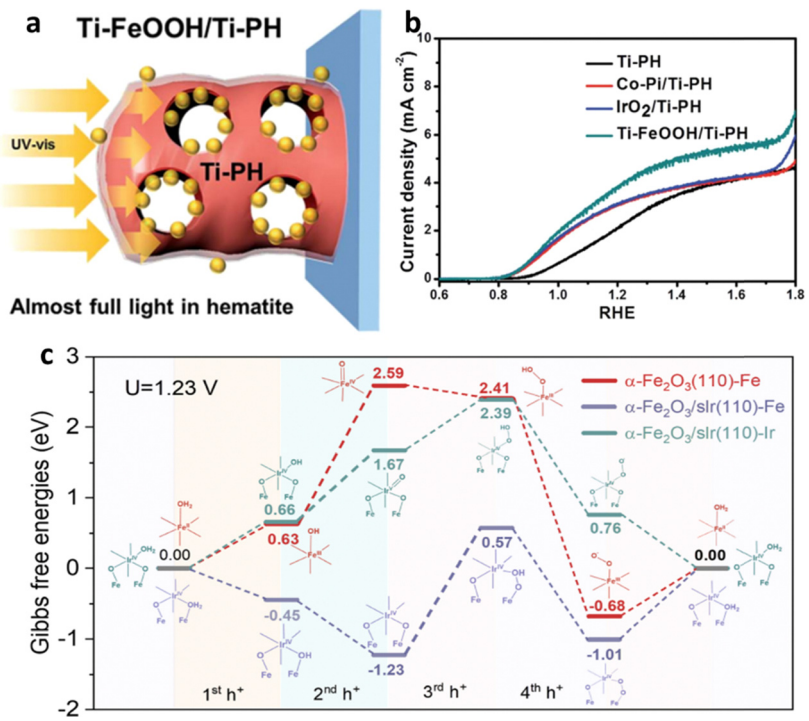

Fig. 21 Impact of catalyst. (a) Effect of Ti-FeOOH cocatalyst decoration on light absorption. (b) Comparative PEC performances of different co-catalysts on Ti-P co-doped hematite. Reproduced from ref. 153 with permission from Royal Society of Chemistry. (c) Energy profiles of α-Fe_2O_3(110), which is represented in red, while the reaction mechanism of α-Fe_2O_3/sIr(110) with Fe as the active site is depicted in purple, and the mechanism with Ir as the sole catalytic site is shown in Nile blue. Reprinted with permission from ref. 156, Copyright 2023 American Chemical Society.

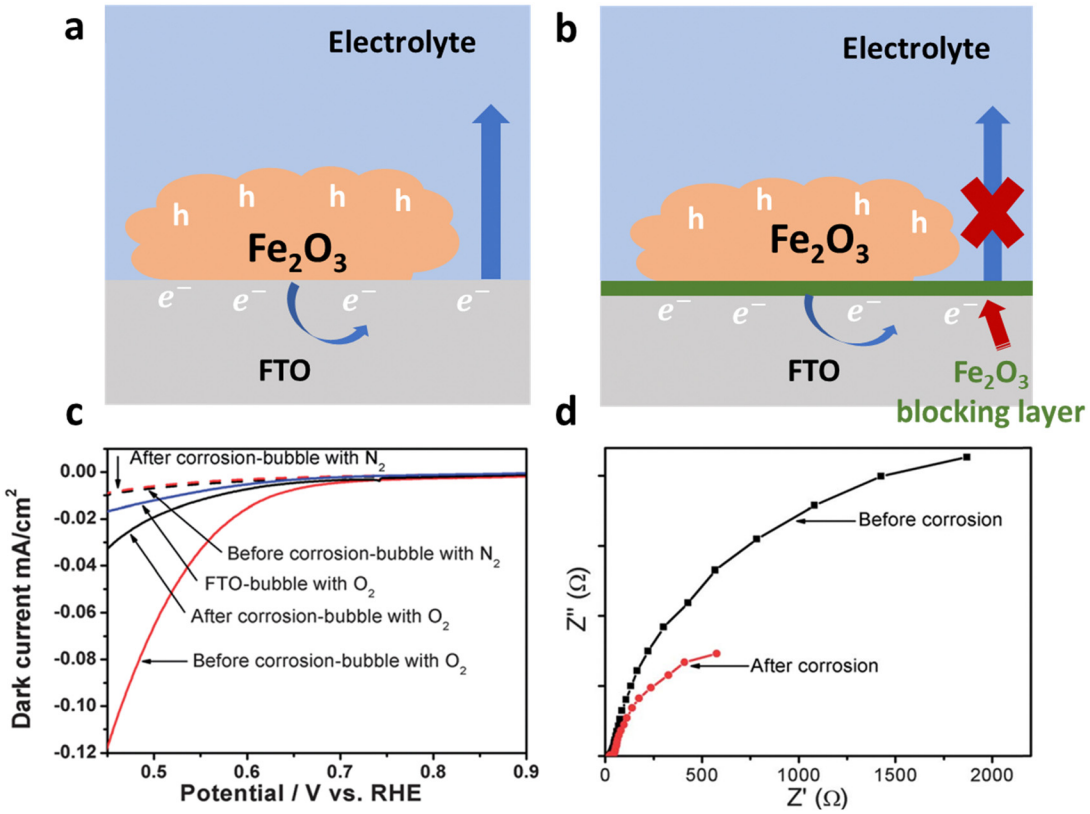

Fig. 22 Schematic of strategies and impact of suppressing the back reaction. (a) Direct contact of a substrate (FTO) with an electrolyte which causes charge separation efficiency loss due to back reactions. (b) Application of a hematite blocking layer which retards the back reaction. (c) Performance of the hematite electrode before and after acid treatment. (d) Charge transfer resistance measurements using EIS before and after corrosion. Reproduced from ref. 160 with permission from Royal Society of Chemistry.

properties by suppressing back reactions and enhancing charge transfer by minimizing the recombination.

Additionally, Zou *et al.*[160] made a notable discovery regarding the enhancement of photocurrent in Ti-doped hematite photoanodes through acid corrosion. Their analysis of dark current, photoluminescence spectroscopy, and transient photocurrent measurements revealed that the increase in photocurrent was not directly linked to improved water oxidation kinetics or surface state passivation. Instead, it was crucial to suppress back reactions. They observed a reduction in dark current in Ti-doped Fe_2O_3 before and after corrosion under different gas-bubbling conditions (N_2 or O_2). When N_2 was bubbled into the electrolyte, the dark current remained negligible. However, after corrosion, a significant decrease in O_2 reduction current was observed in Ti-doped Fe_2O_3 (Fig. 22c), indicating the suppression of the O_2 reduction reaction and confirming the successful suppression of back reactions (Fig. 22d).

5.3.4. Conclusion. Surface charge separation efficiency is crucial for overall STH conversion, but challenges including charge carrier recombination, deficient water oxidation, and undesirable back reactions hinder it. Notably, charge carrier recombination and photovoltage reduction due to surface states and subpar OER are significant issues. Techniques such as sintering, acid/base treatments, and coatings with metal oxides (*e.g.*, TiO_2, Al_2O_3) are employed to address surface state passivation. Innovative approaches, including coating with photoactive materials such as (L)-Cys, offer alternative water oxidation pathways while passivating surface states. Improving water oxidation involves using OER catalysts, but the optimal synergy between hematite's photocatalytic activity and the catalyst is critical for efficiency. Electrocatalysts vary from single atoms to complex structures, and their efficacy depends on interaction with hematite. The photoactive nature of catalysts can further enhance PEC performance by contributing additional electrons and diverse reaction pathways.

6. Summary and outlook

Summary

Hydrogen production through the splitting of water using solar energy is seen as a promising solution to tackle energy and environmental issues. Hematite, a commonly used material for the anode in photoelectrochemical water splitting, is highly regarded due to its abundance, theoretical photocurrent, non-toxic nature, and photochemical stability. However, the practical utilization of hematite photoanodes is currently limited due to several factors such as poor electrical conductivity, and short diffusion length, which cause electron–hole recombination, resulting in low charge separation efficiency. To create an

Table 1 A summarized overview of various known strategies and their impact on hematite

Bulk	Modifications	Strategies	Impact	Remark	Ref.
	Nano-structuring and morphology	3D to 0D confinement	High surface contact		79
			Alter band structure	Reduction in electron–hole recombination	161
			Improves light absorption		162
		Nanowires, nanorods, nano bundles, *etc.*	Shorter hole diffusion path	Less recombination	81
		Matching particle size with hole diffusion length	High charge density Less bulk recombination	Low charge transfer resistance	82
		Branching	Reduces hole drift distance	Improved charge transfer	163
		Making structure porous	Increases area of absorption and contact Reduces the migration distance of charge	Low recombination rate	87
	Doping	Metal	Charge separation and movement through polaron size management	Improved conductivity leads to high charge separation efficiency	164
			Improved carrier density Drift velocity improvement Band bending/built-in field		165
		Semiconductor/nonmetal	Reduces the electron–hole recombination center Generates an internal electric field for easy hole extraction	Built-in field and reduction in recombination center improve charge transfer	99 96
		Multi-element doping	Passivation of surface state and grain boundaries	Multiple modifications	166
			Improvement in charge carrier density		125
			Suppressing agglomeration		167
Interface	H/Substrate	Metal oxide coating	Provide conformal contact	Reduces the contact resistance	168
			Provide control on the growth of H Reduces defects of surfaces		145
			Improves electrons extraction		146
	H/catalyst	Mxene coating/Polymer base semiconductor coating	Improves the hole extraction Provide conformal contact	Improves catalytic activity	121
			Mitigate surface defects of H and catalyst		120
Surface	Grain boundaries	Metal oxide/element	Reduces grain boundaries recombination center	Improves bulk and surface charge transfer efficiency	124 and 169
	Catalyst	Molecular	Reduction in onset potential	Promoters of hole extraction enhance the activity of a catalyst	170
		Metal oxide	Hole extraction		171
		Perovskite	Passivation of the surface state of H		172
		Metal hydroxide	Improvement in OER kinetics	Reduces the charge transfer resistance	120 and 153
		Single-atom catalyst			156
	Sintering	Annealing	Surface state modulation	Cathodic shift	134
				Low Rct	135
	Acid/base treatment	Acid wash with different dopant	Modifications in surface composition	Photovoltage improvement	131
		Different acid wash			139
		Base treatment	Metal oxygen bond formation	Cathodic shift	140
			Defect and surface state modulation		141

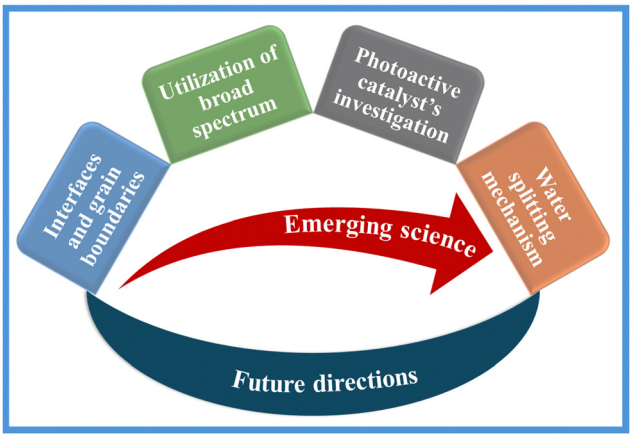

Fig. 23 Schematic of emerging strategies for hematite photoanode.

ideal PEC photoanode, it is crucial to achieve a lower onset potential (close to the flat potential) and a more saturated photocurrent curve (approaching the theoretical photocurrent). This review summarizes the various key strategies used to enhance charge separation efficiency in the bulk, surface, and interface. This review aims to provide a broad understanding of hematite photoanodes with improved charge separation efficiency, leading to enhanced photochemical performance, as summarized in Table 1.

Outlook

For further improvements, the following points could be considered (Fig. 23). According to the machine learning calculations, managing interfacial resistance is crucial; therefore, optimizing interfacial resistance is imperative for enhancing charge transfer efficiency in hematite. Achieving soft and conformal uniform contact between interfaces, addressing electron–hole recombination centers, and dealing with surface states show potential for improved efficiency. Considering the charge extraction property of the contact material can further contribute to enhanced transfer efficiency.

Grain boundaries represent another pivotal consideration, with efforts directed towards minimizing recombination at these sites to elevate both surface and bulk charge separation efficiency. Simultaneously modifying factors such as grain boundaries, surface states, and charge carrier density *via* multi-elemental doping is paramount for approaching the theoretical current density of hematite.

Innovative approaches for different reaction pathways or the utilization of light, such as passivating hematite with photoactive materials like L-cysteine, show potential in providing additional electrons to facilitate water-splitting reactions. Overcoming challenges related to light absorption entails nanostructuring morphology and employing multiple-material electrodes to broaden the spectrum of light absorption.

Catalyst selection is a central theme, with a comprehensive approach aimed at improving charge transfer, oxygen evolution reaction kinetics, surface state passivation, onset potential shift, and photovoltage. Catalysts with photosensitivity, plasmonic characteristics, *etc.*, can further contribute to practical system performance. The exploration of advanced catalyst technologies, including single-atom catalysis, Mxene, *etc.*, is actively shaping the future landscape.

A comprehensive understanding of potential modifications necessitates a clear mechanistic insight. Recently proposed mechanisms, such as the parallel water photooxidation pathways in hematite suggested by Tsyganok *et al.*,[173] offer valuable insights. Unraveling these reaction pathways can pave the way for strategic modifications. Additionally, the full utilization of cocatalyst potential by adding a hole or electron extractor is essential. Beyond modifications, elucidating the underlying mechanisms is crucial for advancing the field and optimizing the performance of hematite-based systems.

Conflicts of interest

The authors declare no conflicts of interest.

Acknowledgements

This work was supported by the National Research Foundation of Korea (NRF) grant funded by the Korean government (MSIT) (No. NRF-2020R1A2C2014050 and NRF-2020R1A5A1019631).

References

1 Michael Grätzel, Photoelectrochemical cells, *Nature*, 2001, **414**, 338–344.
2 S. Du, X. Bian, Y. Zhao, R. Shi and T. Zhang, Progress and Prospect of Photothermal Catalysis, *Chem. Res. Chin. Univ.*, 2022, **38**, 723–734.
3 I. Holmes-Gentle, S. Tembhurne and C. Suter, *et al.*, Kilowatt-scale solar hydrogen production system using a concentrated integrated photoelectrochemical device, *Nat. Energy*, 2023, **8**, 586–596.
4 T. Takata, *et al.*, Photocatalytic Water Splitting with Quantum Efficiency of Almost Unity, *Nature*, 2020, **581**, 411–414.
5 H. Lyu, *et al.*, An Al-doped $SrTiO_3$ photocatalyst maintaining sunlight-driven overall water splitting activity for over 1000 h of constant illumination, *Chem. Sci.*, 2019, **10**, 3196–3201.
6 A. Fujishima and K. Honda, *Nature*, 1972, **238**, 37–38.
7 D. Klotz, D. A. Grave and A. Rothschild, Accurate determination of the charge transfer efficiency of photoanodes for solar water splitting, *Phys. Chem. Chem. Phys.*, 2017, **19**, 20383–20392.
8 X. Zong, *et al.*, A scalable colloidal approach to prepare hematite films for efficient solar water splitting, *Phys. Chem. Chem. Phys.*, 2013, **15**, 12314–12321.
9 P. Dias, A. Vilanova, T. Lopes, L. Andrade and A. Mendes, Extremely stable bare hematite photoanode for solar water splitting, *Nano Energy*, 2016, **23**, 70–79.

10 J. Pina, *et al.*, Phenomenological Understanding of Hematite Photoanode Performance, *J. Phys. Chem. C*, 2021, **125**, 8274–8284.
11 D. Chen, Z. Liu and S. Zhang, Enhanced PEC performance of hematite photoanode coupled with bimetallic oxyhydroxide NiFeOOH through a simple electroless method, *Appl. Catal., B*, 2020, **265**, 118580.
12 D. K. Lee and K. S. Choi, Enhancing long-term photostability of BiVO4 photoanodes for solar water splitting by tuning electrolyte composition, *Nat. Energy*, 2018, **3**, 53–60.
13 J. Zhang, Y. Huang, X. Lu, J. Yang and Y. Tong, Enhanced BiVO4Photoanode Photoelectrochemical Performance *via* Borate Treatment and a NiFeOx Cocatalyst, *ACS Sustainable Chem. Eng.*, 2021, **9**, 8306–8314.
14 W. Fang, L. Fu, A. Qin, Y. Lin and R. Xv, Highly Active and Self-Healing Co-Doped BiVO4Photoanode in Borate Buffer to Enhance Charge Separation and Water Oxidation Kinetics during Photoelectrochemical Water Splitting, *ACS Appl. Energy Mater.*, 2022, **5**(5), 6313–6323.
15 J. Knöppel, *et al.*, Photocorrosion of WO_3 Photoanodes in Different Electrolytes, *ACS Phys. Chem. Au*, 2021, **1**, 6–13.
16 W. L. Kwong, H. Qiu, A. Nakaruk, P. Koshy and C. C. Sorrell, Photoelectrochemical properties of WO_3 thin films prepared by electrodeposition, *Energy Procedia*, 2013, **34**, 617–626.
17 C. Nomellini, *et al.*, Improved Photoelectrochemical Performance of WO 3/BiVO 4 Heterojunction Photoanodes *via* WO 3 Nanostructuring, *ACS Appl. Mater. Interfaces*, 2023, **15**(45), 52436–52447.
18 B. J. Trześniewski and W. A. Smith, Photocharged BiVO4 photoanodes for improved solar water splitting, *J. Mater. Chem. A*, 2016, **4**, 2919–2926.
19 Z. Tian, *et al.*, Novel Black BiVO4/TiO2−x Photoanode with Enhanced Photon Absorption and Charge Separation for Efficient and Stable Solar Water Splitting, *Adv. Energy Mater.*, 2019, **9**(27), 1901287.
20 H. Liu, *et al.*, Hematite-based photoanodes for photoelectrochemical water splitting: Performance, understanding, and possibilities, *J. Environ. Chem. Eng.*, 2023, **11**(1), 109224.
21 G. Liu, *et al.*, Tuning the morphology and structure of disordered hematite photoanodes for improved water oxidation: A physical and chemical synergistic approach, *Nano Energy*, 2018, **53**, 745–752.
22 K. Sivula, F. L. Formal and M. Grätzel, WO_3-Fe_2O_3 photoanodes for water splitting: A host scaffold, guest absorber approach, *Chem. Mater.*, 2009, **21**, 2862–2867.
23 Z. Chen, H. N. Dinh and E. Miller, *Photoelectrochemical water splitting*, Springer, New York, 2013, vol. 344.
24 M. A. Steiner, *et al.*, Photoelectrochemical water splitting using strain-balanced multiple quantum well photovoltaic cells, *Sustainable Energy Fuels*, 2019, **3**, 2837–2844.
25 G. Hodes, Photoelectrochemical cell measurements: Getting the basics right, *J. Phys. Chem. Lett.*, 2012, **3**, 1208–1213.
26 M. Kumar, B. Meena, P. Subramanyam, D. Suryakala and C. Subrahmanyam, Recent trends in photoelectrochemical water splitting: the role of cocatalysts, *NPG Asia Mater.*, 2022, **14**(1), 88.
27 J. Shi, X. Zhao and C. Li, Surface Passivation Engineering for Photoelectrochemical Water Splitting, *Catalysts*, 2023, **13**(2), 217.
28 A. C. Lazanas and M. I. Prodromidis, Electrochemical Impedance Spectroscopy-A Tutorial, *ACS Meas. Sci. Au*, 2023, **3**, 162–193.
29 F.-R. F. Fan and A. J. Bard, *Semiconductor Electrodes XXXVI. Characteristics of n-MoSe s, n-and p-WSe 2 Electrodes in Aqueous Solution*. **https://www.ecsdl.org/terms_use.jsp**.
30 Y. Liu, *et al.*, Enhanced photoelectrocatalytic performance of α-Fe_2O_3 thin films by surface plasmon resonance of Au nanoparticles coupled with surface passivation by atom layer deposition of Al_2O_3, *Nanoscale Res. Lett.*, 2015, **10**, 1–8.
31 K. Sivula, Mott-Schottky analysis of photoelectrodes: Sanity checks are needed, *ACS Energy Lett.*, 2021, **6**, 2549–2551, DOI: **10.1021/acsenergylett.1c01245**.
32 A. Adán-Más, T. M. Silva, L. Guerlou-Demourgues and M. F. Montemor, Application of the Mott-Schottky model to select potentials for EIS studies on electrodes for electrochemical charge storage, *Electrochim Acta*, 2018, **289**, 47–55.
33 M. Förster, D. W. F. Cheung, A. M. Gardner and A. J. Cowan, *Potential and Pitfalls: On the Use of Transient Absorption Spectroscopy for In-Situ and Operando Studies of Photoelectrodes*. (2005).
34 The Current Situation in Ultra-Precision Technology – Silicon Single Crystals as an Example, in *Advances in CMP Polishing Technologies*, ed. T. Doi, I. D. Marinescu and S. Kurokawa, Elsevier, 2012, pp. 15–111.
35 Z. Chen, H. N. Dinh and E. Miller, *Photoelectrochemical water splitting*, Springer, New York, 2013, vol. 344.
36 R. Zeng, C. M. Mannaerts and C. Lievens, Assessment of UV-VIS spectra analysis methods for quantifying the absorption properties of chromophoric dissolved organic matter (CDOM), *Front. Environ. Sci.*, 2023, **11**, 496.
37 W. Zhu, X. Cui, L. Wang, T. Liu and Q. Zhang, Monodisperse porous pod-like hematite: Hydrothermal formation, optical absorbance, and magnetic properties, *Mater. Lett.*, 2011, **65**, 1003–1006.
38 T. Hashimoto, T. Yamada and T. Yoko, Third-order nonlinear optical properties of sol–gel derived α-Fe_2O_3, γ-Fe_2O_3, and Fe_3O_4 thin films, *J. Appl. Phys.*, 1996, **80**, 3184–3190.
39 A. C. Marra, A. Blanco, S. Fonti, A. Jurewicz and V. Orofino, Fine hematite particles of Martian interest: absorption spectra and optical constants, *J. Phys.: Conf. Ser.*, 2005, **6**, 132–138.
40 Y. P. He, *et al.*, Size and structure effect on optical transitions of iron oxide nanocrystals, *Phys. Rev. B: Condens. Matter Mater. Phys.*, 2005, **71**(12), 125411.
41 L. Fang, *et al.*, Experimental and theoretical evidence of enhanced ferromagnetism in sonochemical synthesized $BiFeO_3$ nanoparticles, *Appl. Phys. Lett.*, 2010, **97**, 242501.

42 T. J. LaTempa, X. Feng, M. Paulose and C. A. Grimes, Temperature-dependent growth of self-assembled hematite (α-Fe_2O_3) nanotube arrays: Rapid electrochemical synthesis and photoelectrochemical properties, *J. Phys. Chem. C*, 2009, **113**, 16293–16298.

43 K. Sivula, F. Le Formal and M. Grätzel, Solar water splitting: Progress using hematite (α-Fe 2O3) photoelectrodes, *ChemSusChem*, 2011, **4**, 432–449, DOI: **10.1002/cssc.201000416**.

44 A. G. Joly, *et al.*, Carrier dynamics in α-Fe_2O_3 (0001) thin films and single crystals probed by femtosecond transient absorption and reflectivity, *J. Appl. Phys.*, 2006, **99**, 053521.

45 S. M. Ahmed, J. Leduc and S. F. Haller, Photoelectrochemical and Impedance Characteristics of Specular Hematite. 1. Photoelectrochemical, Parallel Conductance, and Trap Rate Studies Introduction The photoelectrochemical (PEC) properties of a-Fe_2O_3 have been extensively investigated in view of its possible application as a photoanode in the photoelectrolysis of water for hydrogen, *J. Phys. Chem*, 1988, **92**(23), 6655–6660.

46 P. Liao and E. A. Carter, Optical excitations in hematite (α-Fe_2O_3) *via* embedded cluster models: A CASPT2 study, *J. Phys. Chem. C*, 2011, **115**, 20795–20805.

47 D. A. Grave, N. Yatom, D. S. Ellis, M. C. Toroker and A. Rothschild, The ''Rust'' Challenge: On the Correlations between Electronic Structure, Excited State Dynamics, and Photoelectrochemical Performance of Hematite Photoanodes for Solar Water Splitting, *Adv. Mater.*, 2018, **30**(41), 1706577.

48 J. H. Kennedy and W. F. Karl, Photooxidation of water at α-Fe_2O_3 electrodes, *J. Electrochem. Soc.*, 1978, **125**, 709.

49 A. Braun, *et al.*, Direct observation of two electron holes in a hematite photoanode during photoelectrochemical water splitting, *J. Phys. Chem. C*, 2012, **116**, 16870–16875.

50 Z. Zhang and J. T. Yates, Band bending in semiconductors: Chemical and physical consequences at surfaces and interfaces, *Chem. Rev.*, 2012, **112**, 5520–5551.

51 P. Liu, *et al.*, Ultrathin Hematite Photoanode with Gradient Ti Doping, *Research*, 2020, **2020**, 5473217.

52 H. Lüth, *Solid surfaces, interfaces and thin films*, Springer, Berlin, 2001, vol. 4.

53 C. Du, *et al.*, Observation and alteration of surface states of hematite photoelectrodes, *J. Phys. Chem. C*, 2014, **118**, 17054–17059.

54 X. Yang, C. Du, R. Liu, J. Xie and D. Wang, Balancing photovoltage generation and charge-transfer enhancement for catalyst-decorated photoelectrochemical water splitting: A case study of the hematite/MnO_x combination, *J. Catal.*, 2013, **304**, 86–91.

55 J. Wang, W. B. White and J. H. Adair, Optical properties of hydrothermally synthesized hematite particulate pigments, *J. Am. Ceram. Soc.*, 2005, **88**, 3449–3454.

56 L. Chen, *et al.*, Continuous shape- and spectroscopy-tuning of hematite nanocrystals, *Inorg. Chem.*, 2010, **49**, 8411–8420.

57 L. A. Marusak, R. Messier and W. B. White, Optical absorption spectrum of hematite, αFe_2O_3 near IR to UV, *J. Phys. Chem. Solids*, 1980, **41**(9), 981–984.

58 A. Rufus, N. Sreeju and D. Philip, Size tunable biosynthesis and luminescence quenching of nanostructured hematite (α-Fe_2O_3) for catalytic degradation of organic pollutants, *J. Phys. Chem. Solids*, 2019, **124**, 221–234.

59 S. H. Tolbert and A. P. Alivisatos, Size dependence of a first order solid-solid phase transition: the wurtzite to rock salt transformation in CdSe nanocrystals, *Science*, 1994, **265**(5170), 373–376.

60 B. Zou, *et al.*, Anomalous optical properties and electron-phonon coupling enhancement in Fe_2O_3 nanoparticles coated with a layer of stearates, *Phys. Chem. Solids*, 1997, **58**(9), 1315–1320.

61 N. J. Cherepy, D. B. Liston, J. A. Lovejoy, H. Deng and J. Z. Zhang, *Ultrafast Studies of Photoexcited Electron Dynamics in γ-and r-Fe_2O_3 Semiconductor Nanoparticles*, 1998, **https://pubs.acs.org/sharingguidelines**.

62 E. Thimsen, S. Biswas, C. S. Lo and P. Biswas, Predicting the band structure of mixed transition metal oxides: Theory and experiment, *J. Phys. Chem. C*, 2009, **113**, 2014–2021.

63 G. Rollmann, A. Rohrbach, P. Entel and J. Hafner, First-principles calculation of the structure and magnetic phases of hematite, *Phys. Rev. B: Condens. Matter Mater. Phys.*, 2004, **69**(16), 165107.

64 T. Droubay, *et al.*, Structure, magnetism, and conductivity in epitaxial Ti-doped α-Fe_2O_3 hematite: Experiment and density functional theory calculations, *Phys. Rev. B: Condens. Matter Mater. Phys.*, 2007, **75**(10), 104412.

65 F. Le Formal, *et al.*, Rate Law Analysis of Water Oxidation on a Hematite Surface, *J. Am. Chem. Soc.*, 2015, **137**, 6629–6637.

66 Y. Zhang, *et al.*, Rate-Limiting O–O Bond Formation Pathways for Water Oxidation on Hematite Photoanode, *J. Am. Chem. Soc.*, 2018, **140**, 3264–3269.

67 Y. Zhang, *et al.*, Pivotal Role and Regulation of Proton Transfer in Water Oxidation on Hematite Photoanodes, *J. Am. Chem. Soc.*, 2016, **138**, 2705–2711.

68 K. Y. Yoon, *et al.*, Hematite-based photoelectrochemical water splitting supported by inverse opal structures of graphene, *ACS Appl. Mater. Interfaces*, 2014, **6**, 22634–22639.

69 I. Cesar, K. Sivula, A. Kay, R. Zboril and M. Grätzel, Influence of Feature Size, Film Thickness, and Silicon Doping on the Performance of Nanostructured Hematite Photoanodes for Solar Water Splitting, *J. Phys. Chem. C*, 2009, **113**, 772–782.

70 J. J. Wang, Y. Hu, R. Toth, G. Fortunato and A. Braun, A facile nonpolar organic solution process of a nanostructured hematite photoanode with high efficiency and stability for water splitting, *J. Mater. Chem. A*, 2016, **4**, 2821–2825.

71 L. Liardet, J. E. Katz, J. Luo, M. Grätzel and X. Hu, An ultrathin cobalt-iron oxide catalyst for water oxidation on nanostructured hematite photoanodes, *J. Mater. Chem. A*, 2019, **7**, 6012–6020.

72 K. T. C. Thomaz, *et al.*, Interfacial engineering of hematite photoanodes toward high water splitting performance, *Mater Today Energy*, 2023, **37**, 101399.

73 Y. Lin, S. Zhou, S. W. Sheehan and D. Wang, Nanonet-Based hematite heteronanostructures for efficient solar water splitting, *J. Am. Chem. Soc.*, 2011, **133**, 2398–2401.

74 J. Y. Kim, *et al.*, Single-crystalline, wormlike hematite photoanodes for efficient solar water splitting, *Sci. Rep.*, 2013, **3**(1), 2681.
75 P. Peerakiatkhajohn, *et al.*, Stable Hematite Nanosheet Photoanodes for Enhanced Photoelectrochemical Water Splitting, *Adv. Mater.*, 2016, **28**, 6405–6410.
76 A. J. E. Rettie, W. D. Chemelewski, D. Emin and C. B. Mullins, Unravelling Small-Polaron Transport in Metal Oxide Photoelectrodes, *J. Phys. Chem. Lett.*, 2016, **7**, 471–479, DOI: **10.1021/acs.jpclett.5b02143**.
77 L. M. Carneiro, *et al.*, Excitation-wavelength-dependent small polaron trapping of photoexcited carriers in α-Fe_2O_3, *Nat. Mater.*, 2017, **16**, 819–825.
78 K. Yan, *et al.*, Self-driven hematite-based photoelectrochemical water splitting cells with three-dimensional nanobowl heterojunction and high-photovoltage perovskite solar cells, *Mater Today Energy*, 2017, **6**, 128–135.
79 A. Tofanello, S. Shen, F. L. De Souza and L. Vayssieres, Strategies to improve the photoelectrochemical performance of hematite nanorod-based photoanodes, *APL Mater.*, 2020, **8**(4), 040905.
80 X. Yang, *et al.*, Ordered mesoporous ZnGa2O4for photocatalytic hydrogen evolution, *Mater. Chem. Front.*, 2021, **5**, 5790–5797.
81 J. Wang, *et al.*, Facile Synthesis of Ultrafine Hematite Nanowire Arrays in Mixed Water-Ethanol-Acetic Acid Solution for Enhanced Charge Transport and Separation, *ACS Appl. Mater. Interfaces*, 2018, **10**, 12594–12602.
82 Z. Zhang, H. Nagashima and T. Tachikawa, Ultra-Narrow Depletion Layers in a Hematite Mesocrystal-Based Photoanode for Boosting Multihole Water Oxidation, *Angew. Chem., Int. Ed.*, 2020, **59**, 9047–9054.
83 Z. Luo, *et al.*, Dendritic Hematite Nanoarray Photoanode Modified with a Conformal Titanium Dioxide Interlayer for Effective Charge Collection, *Angew. Chem.*, 2017, **129**, 13058–13062.
84 K. Y. Yoon, *et al.*, Unveiling the Role of the Ti Dopant and Viable Si Doping of Hematite for Practically Efficient Solar Water Splitting, *ACS Catal.*, 2022, **12**, 5112–5122.
85 C. H. Bak, K. Kim, K. Jung, J. B. Kim and J. H. Jang, Efficient photoelectrochemical water splitting of nanostructured hematite on a three-dimensional nanoporous metal electrode, *J. Mater. Chem. A*, 2014, **2**, 17249–17252.
86 H. Ahn, K. Yoon, M. Kwak and J. Jang, A Titanium-Doped SiO_x Passivation Layer for Greatly Enhanced Performance of a Hematite-Based Photoelectrochemical System, *Angew. Chem.*, 2016, **128**, 10076–10080.
87 K. Y. Yoon, *et al.*, Unveiling the Role of the Ti Dopant and Viable Si Doping of Hematite for Practically Efficient Solar Water Splitting, *ACS Catal.*, 2022, **12**, 5112–5122.
88 T. H. Jeon, H. I. Cho, H. Park, H. Kim and W. Choi, Synergistic effect of Sn doping and hydrogenation on hematite electrodes for photoelectrochemical water oxidation, *Mater. Chem. Front.*, 2021, **5**, 6592–6602.
89 J. Deng, *et al.*, Ti-doped hematite nanostructures for solar water splitting with high efficiency, *J. Appl. Phys.*, 2012, **112**(8), 084312.
90 P. Kumar, P. Sharma, R. Shrivastav, S. Dass and V. R. Satsangi, Electrodeposited zirconium-doped α-Fe_2O_3 thin film for photoelectrochemical water splitting, *Int. J. Hydrogen Energy*, 2011, **36**, 2777–2784.
91 Y. Ling, G. Wang, D. A. Wheeler, J. Z. Zhang and Y. Li, Sn-doped hematite nanostructures for photoelectrochemical water splitting, *Nano Lett.*, 2011, **11**, 2119–2125.
92 C. Xiao, Z. Zhou, L. Li, S. Wu and X. Li, Tin and Oxygen-Vacancy Co-doping into Hematite Photoanode for Improved Photoelectrochemical Performances, *Nanoscale Res. Lett.*, 2020, **15**, 54.
93 A. Annamalai, *et al.*, Activation of hematite photoanodes for solar water splitting: Effect of FTO deformation, *J. Phys. Chem. C*, 2015, **119**, 3810–3817.
94 J. Park, *et al.*, A highly transparent thin film hematite with multi-element dopability for an efficient unassisted water splitting system, *Nano Energy*, 2020, **76**, 105089.
95 L. M. Daminelli, *et al.*, Self-Diffusion versus Intentional Doping: Beneficial and Damaging Impact on Hematite Photoanode Interfaces, *ACS Appl. Mater. Interfaces*, 2023, **15**(47), 55030–55042.
96 H. J. Ahn, K. Y. Yoon, M. J. Kwak, J. Park and J. H. Jang, Boron Doping of Metal-Doped Hematite for Reduced Surface Recombination in Water Splitting, *ACS Catal.*, 2018, **8**, 11932–11939.
97 Y. Zhang, *et al.*, Nonmetal P-doped hematite photoanode with enhanced electron mobility and high water oxidation activity, *Energy Environ. Sci.*, 2015, **8**, 1231–1236.
98 Z. Luo, C. Li, S. Liu, T. Wang and J. Gong, Gradient doping of phosphorus in Fe_2O_3 nanoarray photoanodes for enhanced charge separation, *Chem. Sci.*, 2016, **8**, 91–100.
99 J. Kang, *et al.*, Meso-pore generating P doping for efficient photoelectrochemical water splitting, *Nano Energy*, 2023, **107**, 108090.
100 K. Y. Yoon, *et al.*, NiFeOx decorated Ge-hematite/perovskite for an efficient water splitting system, *Nat. Commun.*, 2021, **12**(1), 4309.
101 K. Kim, I. H. Kim, K. Y. Yoon, J. Lee and J. H. Jang, α-Fe_2O_3 on patterned fluorine doped tin oxide for efficient photoelectrochemical water splitting, *J. Mater. Chem. A*, 2015, **3**, 7706–7709.
102 D. Chen and Z. Liu, Dual-Axial Gradient Doping (Zr and Sn) on Hematite for Promoting Charge Separation in Photoelectrochemical Water Splitting, *ChemSusChem*, 2018, **11**, 3438–3448.
103 L. Li, *et al.*, New method for improving the bulk charge separation of hematite with enhanced water splitting, *Int. J. Hydrogen Energy*, 2019, **44**, 4208–4217.
104 A. Tofanello, *et al.*, Hematite Surface Modification toward Efficient Sunlight-Driven Water Splitting Activity: The Role of Gold Nanoparticle Addition, *J. Phys. Chem. C*, 2020, **124**(11), 6171–6179.
105 F. Li, *et al.*, Facile regrowth of Mg-Fe_2O_3/P-Fe_2O_3 homojunction photoelectrode for efficient solar water oxidation, *J. Mater. Chem. A*, 2018, **6**, 13412–13418.
106 Z. Zheng, X. Zu, Y. Zhang and W. Zhou, Rational design of type-II nano-heterojunctions for nanoscale optoelectronics, *Mater. Today Phys.*, 2020, **15**, 100262.

107 S. Li, W. Xu, L. Meng, W. Tian and L. Li, Recent Progress on Semiconductor Heterojunction-Based Photoanodes for Photoelectrochemical Water Splitting, *Small Science*, 2022, **2**, 2100112.
108 J. Leduc, *et al.*, Electronically Coupled Uranium and Iron Oxide Heterojunctions as Efficient Water Oxidation Catalysts, *Adv. Funct. Mater.*, 2019, **29**(50), 1905005.
109 H. Zhang, Y. K. Kim, H. Y. Jeong and J. S. Lee, A Few Atomic $FeNbO_4$ Overlayers on Hematite Nanorods: Microwave-Induced High Temperature Phase for Efficient Photoelectrochemical Water Splitting, *ACS Catal.*, 2019, **9**, 1289–1297.
110 Y. Hu, *et al.*, Molecular Origin and Electrochemical Influence of Capacitive Surface States on Iron Oxide Photoanodes, *J. Phys. Chem. C*, 2016, **120**, 3250–3258.
111 M. Pyeon, *et al.*, Critical role and modification of surface states in hematite films for enhancing oxygen evolution activity, *J. Mater. Res.*, 2018, **33**, 455–466.
112 T. Idei, Y. Nagai, Z. Pan and K. Katayama, Identification of the Contributing Factors to the Photoelectric Conversion Efficiency for Hematite Photoanodes by Using Machine Learning, *ACS Appl. Mater. Interfaces*, 2023, **15**(48), 55644–55651.
113 X. Li, P. S. Bassi, P. P. Boix, Y. Fang and L. H. Wong, Revealing the Role of TiO_2 Surface Treatment of Hematite Nanorods Photoanodes for Solar Water Splitting, *ACS Appl. Mater. Interfaces*, 2015, **7**, 16960–16966.
114 D. Wang, *et al.*, Boosting photoelectrochemical performance of hematite photoanode with TiO_2 underlayer by extremely rapid high temperature annealing, *Appl. Surf. Sci.*, 2017, **422**, 913–920.
115 J. Wang, B. Feng, J. Su and L. Guo, Enhanced bulk and interfacial charge transfer dynamics for efficient photoelectrochemical water splitting: The case of hematite nanorod arrays, *ACS Appl. Mater. Interfaces*, 2016, **8**, 23143–23150.
116 F. Li, *et al.*, TiO_2 passivation layers with laser derived p-n heterojunctions enable boosted photoelectrochemical performance of α-Fe_2O_3 photoanodes, *Chem. Eng. J.*, 2023, **461**, 141872.
117 L. Steier, *et al.*, Understanding the role of underlayers and overlayers in thin film hematite photoanodes, *Adv. Funct. Mater.*, 2014, **24**, 7681–7688.
118 T. Hisatomi, *et al.*, Enhancement in the performance of ultrathin hematite photoanode for water splitting by an oxide underlayer, *Adv. Mater.*, 2012, **24**, 2699–2702.
119 M. Li, *et al.*, Zipping up NiFe(OH)x-Encapsulated Hematite to Achieve an Ultralow Turn-On Potential for Water Oxidation, *ACS Energy Lett.*, 2019, **4**, 1983–1990.
120 J. Park, *et al.*, Boosting Charge Transfer Efficiency by Nanofragment MXene for Efficient Photoelectrochemical Water Splitting of $NiFe(OH)_x$ Co-Catalyzed Hematite, *ACS Appl. Mater. Interfaces*, 2023, **15**(7), 9341–9349.
121 H. J. Ahn, *et al.*, Utilizing a Siloxane-Modified Organic Semiconductor for Photoelectrochemical Water Splitting, *ACS Energy Lett.*, 2023, 2595–2602, DOI: **10.1021/acsenergylett.3c00755**.
122 F. C. De Lima, *et al.*, Unveiling the dopant segregation effect at hematite interfaces, *Appl. Phys. Lett.*, 2021, **118**(20), 201602.
123 M. R. S. Soares, *et al.*, Unraveling the Role of Sn Segregation in the Electronic Transport of Polycrystalline Hematite: Raising the Electronic Conductivity by Lowering the Grain-Boundary Blocking Effect, *Adv. Electron. Mater.*, 2019, **5**(6), 1900065.
124 F. Feng, *et al.*, Boosting hematite photoelectrochemical water splitting by decoration of TiO_2 at the grain boundaries, *Chem. Eng. J.*, 2019, **368**, 959–967.
125 F. A. Pires, *et al.*, Selective placement of modifiers on hematite thin films for solar water splitting, *Sustainable Energy Fuels*, 2023, **7**(20), 5005–5017.
126 M. P. Cardona, *et al.*, The role of graphene as an overlayer on nanostructured hematite photoanodes for improved solar water oxidation, *Mater. Today Energy*, 2018, **8**, 8–14.
127 J. E. Thorne, S. Li, C. Du, G. Qin and D. Wang, Energetics at the Surface of Photoelectrodes and Its Influence on the Photoelectrochemical Properties, *J. Phys. Chem. Lett.*, 2015, **6**, 4083–4088.
128 M. Barroso, *et al.*, Dynamics of photogenerated holes in surface modified α-Fe_2O_3 photoanodes for solar water splitting, *Proc. Natl. Acad. Sci. U. S. A.*, 2012, **109**, 15640–15645.
129 J. W. Jang, *et al.*, Enabling unassisted solar water splitting by iron oxide and silicon, *Nat. Commun.*, 2015, **6**(1), 7447.
130 J. Xiao, *et al.*, Suppressing the electron–hole recombination rate in hematite photoanode with a rapid cooling treatment, *J. Catal.*, 2017, **350**, 48–55.
131 Q. Wu, *et al.*, Acid-treated Ti_{4+} doped hematite photoanode for efficient solar water oxidation—Insight into surface states and charge separation, *J. Alloys Compd.*, 2019, **782**, 943–951.
132 G. Liu, *et al.*, Tuning the morphology and structure of disordered hematite photoanodes for improved water oxidation: A physical and chemical synergistic approach, *Nano Energy*, 2018, **53**, 745–752.
133 R. Morrish, M. Rahman, J. M. D. MacElroy and C. A. Wolden, Activation of hematite nanorod arrays for photoelectrochemical water splitting, *ChemSusChem*, 2011, **4**, 474–479.
134 O. Zandi and T. W. Hamann, Enhanced water splitting efficiency through selective surface state removal, *J. Phys. Chem. Lett.*, 2014, **5**, 1522–1526.
135 W. Si, F. Haydous, U. Babic, D. Pergolesi and T. Lippert, Suppressed Charge Recombination in Hematite Photoanode *via* Protonation and Annealing, *ACS Appl. Energy Mater.*, 2019, **2**, 5438–5445.
136 P. Y. Tang, *et al.*, Boosting Photoelectrochemical Water Oxidation of Hematite in Acidic Electrolytes by Surface State Modification, *Adv. Energy Mater.*, 2019, **9**(34), 1901836.
137 L. Xi and K. M. Lange, Surface modification of hematite photoanodes for improvement of photoelectrochemical performance, *Catalysts*, 2018, **8**(11), 497.

138 F. Le Formal, K. Sivula and M. Grätzel, The transient photocurrent and photovoltage behavior of a hematite photoanode under working conditions and the influence of surface treatments, *J. Phys. Chem. C*, 2012, **116**, 26707–26720.
139 Y. Yang, *et al.*, Acid Treatment Enables Suppression of Electron-Hole Recombination in Hematite for Photoelectrochemical Water Splitting, *Angew. Chem.*, 2016, **128**, 3464–3468.
140 Y. Wang, J. Liu, J. Xu and X. Hao, Effect of acid treatment on boosting the photoelectrochemical performance of doped and codoped α-Fe_2O_3 photoanodes, *RSC Adv.*, 2023, **13**, 16765–16772.
141 X. Zhang, X. Wang, X. Yi, J. Ye and D. Wang, Alkali Treatment for Enhanced Photoelectrochemical Water Oxidation on Hematite Photoanode, *ACS Sustainable Chem. Eng.*, 2019, **7**, 5420–5429.
142 L. Steier, *et al.*, Understanding the role of underlayers and overlayers in thin film hematite photoanodes, *Adv. Funct. Mater.*, 2014, **24**, 7681–7688.
143 M. G. Ahmed, *et al.*, A Facile Surface Passivation of Hematite Photoanodes with TiO_2 Overlayers for Efficient Solar Water Splitting, *ACS Appl. Mater. Interfaces*, 2015, **7**, 24053–24062.
144 F. Le Formal, *et al.*, Passivating surface states on water splitting hematite photoanodes with alumina overlayers, *Chem. Sci.*, 2011, **2**, 737–743.
145 M. G. Ahmed, *et al.*, A Facile Surface Passivation of Hematite Photoanodes with TiO_2 Overlayers for Efficient Solar Water Splitting, *ACS Appl. Mater. Interfaces*, 2015, **7**, 24053–24062.
146 F. Le Formal, *et al.*, Passivating surface states on water splitting hematite photoanodes with alumina overlayers, *Chem. Sci.*, 2011, **2**, 737–743.
147 L. Zhu, *et al.*, A highly efficient hematite photoelectrochemical fuel cell for solar-driven hydrogen production, *Int. J. Hydrogen Energy*, 2023, **48**, 32699–32707.
148 K. Y. Yoon, *et al.*, A selectively decorated Ti-FeOOH cocatalyst for a highly efficient porous hematite-based water splitting system, *J. Mater. Chem. A*, 2016, **4**, 18730–18736.
149 C. Lo Vecchio, *et al.*, Enhanced photoelectrochemical water splitting at hematite photoanodes by effect of a nife-oxide co-catalyst, *Catalysts*, 2020, **10**(5), 525.
150 M. G. Ahmed, M. Zhang, Y. F. Tay, S. Y. Chiam and L. H. Wong, Surface Modification of Hematite Photoanodes with CeO_x Cocatalyst for Improved Photoelectrochemical Water Oxidation Kinetics, *ChemSusChem*, 2020, **13**, 5489–5496.
151 Z. Wang, *et al.*, Exceptional alkaline hydrogen evolution by molybdenum-oxide-nitride-based electrocatalysts with fast water-dissociation and hydrogen-adsorption kinetics, *Mater. Chem. Front.*, 2023, **7**, 2683–2692.
152 W. Li, *et al.*, Comparison of heterogenized molecular and heterogeneous oxide catalysts for photoelectrochemical water oxidation, *Energy Environ. Sci.*, 2016, **9**, 1794–1802.
153 K. Y. Yoon, *et al.*, A selectively decorated Ti-FeOOH cocatalyst for a highly efficient porous hematite-based water splitting system, *J. Mater. Chem. A*, 2016, **4**, 18730–18736.
154 Z. Lin, *et al.*, Anchoring Single Nickel Atoms on Carbon-vacant Carbon Nitride Nanosheets for Efficient Photocatalytic Hydrogen Evolution, *Chem. Res. Chin. Univ.*, 2022, **38**, 1243–1250.
155 Z. Teng, H. Yang, Q. Zhang and T. Ohno, Carrier Dynamics and Surface Reaction Boosted by Polymer-based Single-atom Photocatalysts, *Chem. Res. Chin. Univ.*, 2022, **38**, 1207–1218.
156 Q. Guo, *et al.*, Single-Atom Iridium on Hematite Photoanodes for Solar Water Splitting: Catalyst or Spectator?, *J. Am. Chem. Soc.*, 2023, **145**, 1686–1695.
157 S. Pokrant, S. Dilger, S. Landsmann and M. Trottmann, Size effects of cocatalysts in photoelectrochemical and photocatalytic water splitting, *Mater. Today Energy*, 2017, **5**, 158–163.
158 T. Hisatomi, *et al.*, Enhancement in the performance of ultrathin hematite photoanode for water splitting by an oxide underlayer, *Adv. Mater.*, 2012, **24**, 2699–2702.
159 F. Bouhjar, B. Bessaïs and B. Marí, Ultrathin-layer α-Fe_2O_3 deposited under hematite for solar water splitting, *J. Solid State Electrochem.*, 2018, **22**, 2347–2356.
160 D. Cao, *et al.*, Cathodic shift of onset potential for water oxidation on a Ti4+ doped Fe_2O_3 photoanode by suppressing the back reaction, *Energy Environ. Sci.*, 2014, **7**, 752–759.
161 Y. H. Chen and C. C. Lin, Effect of nano-hematite morphology on photocatalytic activity, *Phys. Chem. Miner.*, 2014, **41**, 727–736.
162 S. Rehman, *et al.*, Morphological evaluation of hematite nanostructures and their shape dependent photocatalytic and magnetic properties, *Chem. Eng. Process.*, 2022, **175**, 108909.
163 Z. Luo, *et al.*, Dendritic Hematite Nanoarray Photoanode Modified with a Conformal Titanium Dioxide Interlayer for Effective Charge Collection, *Angew. Chem.*, 2017, **129**, 13058–13062.
164 M. Henrique de Matos Rodrigues, *et al.*, Ideal dopant to increase charge separation efficiency in hematite photoanodes: germanium, *J. Mater. Chem. A*, 2022, **10**, 13456–13466.
165 X. Zhang, H. Li, S. Wang, F. R. F. Fan and A. J. Bard, Improvement of hematite as photocatalyst by doping with tantalum, *J. Phys. Chem. C*, 2014, **118**, 16842–16850.
166 L. K. Dhandole, *et al.*, Enhanced charge transfer with tuning surface state in hematite photoanode integrated by niobium and zirconium co-doping for efficient photoelectrochemical water splitting, *Appl. Catal., B*, 2022, **315**, 121538.
167 K. Kang, H. Zhang, J. H. Kim, W. J. Byun and J. S. Lee, An *in situ* fluorine and *ex situ* titanium two-step co-doping strategy for efficient solar water splitting by hematite photoanodes, *Nanoscale Adv.*, 2022, **4**, 1659–1667.
168 Z. Zhou, *et al.*, Understanding the varying mechanisms between the conformal interlayer and overlayer in the silicon/hematite dual-absorber photoanode for solar water splitting, *Dalton Trans.*, 2021, **50**, 2936–2944.

169 M. R. S. Soares, *et al.*, Understanding the fundamental electrical and photoelectrochemical behavior of a hematite photoanode, *Phys. Chem. Chem. Phys.*, 2016, **18**, 21780–21788.
170 A. Tsyganok, D. Klotz, K. D. Malviya, A. Rothschild and D. A. Grave, Different Roles of $Fe_{1-x}Ni_xOOH$ Cocatalyst on Hematite (α-Fe_2O_3) Photoanodes with Different Dopants, *ACS Catal.*, 2018, **8**, 2754–2759.
171 X. S. Xing, *et al.*, Synergy between Mn and Co in Mn/CoO_x cocatalyst for enhanced photoelectrochemical water oxidation of hematite photoanode, *Appl. Surf. Sci.*, 2022, **572**, 151472.
172 Z. Pan, S. Chen and K. Katayama, Roles of Surface States in Cocatalyst-Loaded Hematite Photoanodes for Water Oxidation, *J. Phys. Chem. C*, 2023, **127**(7), 3904–3909.
173 A. Tsyganok, P. Monroy-Castillero, Y. Piekner, A. Yochelis and A. Rothschild, Parallel water photo-oxidation reaction pathways in hematite photoanodes: implications for solar fuel production, *Energy Environ. Sci.*, 2022, **15**, 2445–2459.